minerals

MDPI

Article

Geochemistry, Zircon U-Pb Geochronology and Hf-O Isotopes of the Banzhusi Granite Porphyry from the Xiong'ershan Area, East Qinling Orogen, China: Implications for Petrogenesis and Geodynamics

Bin Wang [1,2,3], Xinkai Hu [3,4,*], Li Tang [3,4] and Jingchao Li [1,2]

1 Development and Research Center, China Geological Survey, Beijing 100037, China
2 National Geological Archives, Beijing 100037, China
3 School of Earth Sciences and Resources, China University of Geosciences Beijing, Beijing 100083, China
4 State Key Laboratory of Geological Processes and Mineral Resources, China University of Geosciences Beijing, Beijing 100083, China
* Correspondence: hxk199203@cugb.edu.cn

Received: 21 July 2019; Accepted: 3 September 2019; Published: 5 September 2019

Abstract: The Banzhusi granite porphyry is located in the Xiong'ershan area, East Qinling orogenic belt (EQOB). This study presents an integrated whole-rock geochemistry and zircon U-Pb-Hf-O isotope analysis of the Banzhusi granite porphyry. These rocks have metaluminous, high-K alkali-calcic and shoshonitic features and show significant enrichment in light rare earth elements (LREEs) over heavy rare earth elements (HREEs) with negative Eu anomalies. These samples are also greatly enriched in Rb, Ba, K, Pb, Th and U and depleted in Nb, Ta, P and Ti, and they mostly overlap the ranges of the Taihua Group tonalite–trondhjemite–granodiorite (TTG) gneiss. Magmatic zircons from three samples of the Banzhusi granite porphyry yield U-Pb ages of 125.1 ± 0.97 Ma, 128.1 ± 1.2 Ma and 128.2 ± 1.3 Ma. The Hf-O isotope features of zircons from the three samples are very similar ($\delta^{18}O_{zircon}$ = 4.84‰ to 6.51‰, $\varepsilon Hf_{(t)}$ = −26.9 to −14.4). The co-variations of geochemical and isotopic data in these granite porphyries imply that the Banzhusi granite porphyry resulted from the mixing of the partially melted Taihua Group and mantle-derived material in a post-collisional setting from 128–125 Ma.

Keywords: geochemistry; zircon U-Pb geochronology; zircon Hf-O isotopes; Banzhusi granite porphyry; East Qinling

1. Introduction

In the East Qinling orogenic belt (EQOB), late Mesozoic granitoid plutons are widely distributed (Figure 1) [1–4]. Most late Mesozoic granitoids are spatially, temporally and genetically correlated with Mo, Au and Ag-Pb-Zn mineralization in the EQOB [2,5–7]. However, the petrogenesis and magma source of these Late Jurassic to Early Cretaceous granitoids remain under debate. The diverse sources of late Mesozoic magmatism include (1) a mixture between partial melting of the lower crust or Archaean-Palaeoproterozoic metamorphic crystalline basement of the North China Craton (NCC) and mantle material [8–12] and (2) partial melting of continental crust of the Yangtze Craton (YC) that subducted beneath the southern margin of the NCC [13–16]. The Banzhusi granite porphyry is located in the eastern part and represents the largest intrusion in the eastern Xiong'ershan area. Previous studies have shown that the Banzhusi granite porphyry was formed at 129 Ma, which correspond to Late JurassicEarly Cretaceous magmatic activity [17,18]. The Banzhusi granite porphyry shows C-type adakitic features with high Sr and low Yb and Y, which indicates that the magma source originated from

partial melting of the thickened crust [17]. However, much previous evidence has suggested that the late Mesozoic magmatism in the Xiong'ershan area was the product of crust-mantle interactions [8,12,19]. Whether the Banzhusi granite porphyry has the same magma sources with the input of mantle materials is unknown.

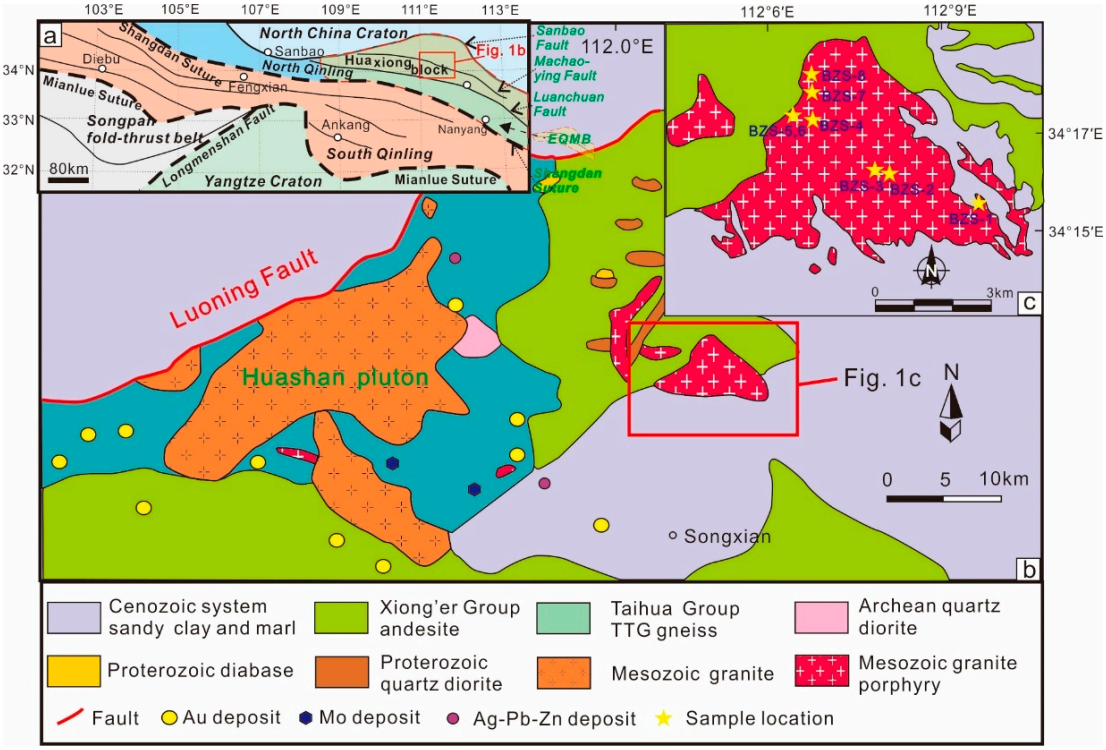

Figure 1. Tectonic framework of the Qinling orogen (**a**), geology and distribution of intrusions in the Xiong'ershan area (**b**) and geological map of the Banzhusi granite porphyry (**c**) (Modified after [17,18,20–24]).

Zircon is a common accessory mineral that can forcefully resist the effects of later geological activities. Therefore, zircon U-Pb-Hf-O isotopes provide insights into the emplacement ages, the magma sources, the physico-chemical conditions of magma and the petrogenetic processes of granitoids [25,26]. In the present study, we measured the whole-rock geochemistry and in situ zircon U-Pb-Hf-O isotopes for the Banzhusi granite porphyry from the Xiong'ershan area in order to (1) precisely determine the emplacement ages of the granite porphyry and (2) decipher the magma source, petrogenesis and tectonic implications.

2. Geological Setting

The Xiong'ershan area is situated along the border of the North Qingling Belt and the Huaxiong Blockin the Qinling orogenic belt (QOB) [27] and consists of two lithospheric units (late Neoarchean-Palaeoproterozoic Taihua Group and Palaeoproterozoic Xiong'er Group, Figure 1) [20,28]. A suite of biotite-plagioclase gneisses, plagioclase-amphibole gneisses, amphibolites, granulites and quartz schists constitute the Taihua Group [29–34]. The Xiong'er Group has been classified as a low-grade, low-strain metamorphosed volcanic sequence that unconformably overlies the Taihua Group, and its lithology consists of basaltic andesite and andesite, with minor dacite and rhyolite [35–42]. In the Xiong'ershan area, magmatic events can be divided into three periods: (i) Palaeoproterozoic magmatism represented by the Xiong'er Group volcanic rocks [39]; (ii) Triassic alkaline magmatism that formed the Mogou granite porphyry, which is exposed as several elliptic syenite stocks [28]; (iii) late Mesozoic magmatism is the most important magmatic event mainly exposed as granite plutons and granite porphyries (Figure 1b) [21]. Late Mesozoic magmatism is closely associated with the

most important regional metallogenic events, including orogenic gold lode deposits [43,44]; porphyry, quartz-vein and carbonatite-vein Mo deposits [45–48]; breccia pipe-hosted gold deposits [49–51]; and hydrothermal vein-type Au and Ag-Pb-Zn deposits [52,53].

The Banzhusi granite porphyry occupies approximately 31 km^2 and mainly intruded into the Paleoproterozoic Xiong'er Group (Figure 1c). The southern and southeastern parts of the Banzhusi granite porphyry are covered by Cenozoic sandy clays and marls. The Banzhusi granite porphyry is grey or light red in color with a typical porphyritic texture. The phenocrysts of granite porphyry mainly consist of 25–40% quartz, plagioclase and K-feldspar. The matrix minerals are made up of quartz (15–30%), plagioclase (10–20%), amphibole (5%) and biotite (<5%). The accessory minerals present a consistent suite that includes magnetite, apatite, titanite, zircon and pyrite (Figure 2).

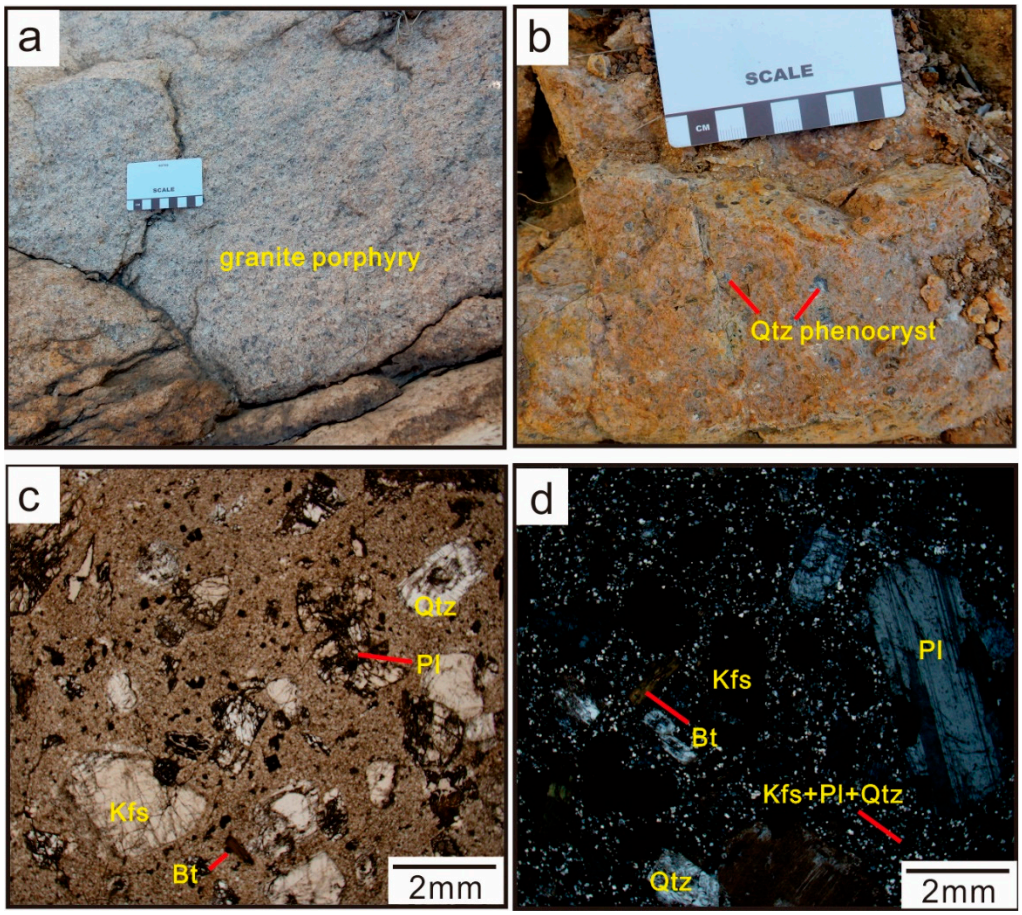

Figure 2. Photographs of representative samples from the Banzhusi granite porphyry. (**a**,**b**) Macroscopic Banzhusi granite porphyry with quartz, plagioclase and K-feldspar phenocrysts. (**c**) Photomicrographs of the granite porphyry, showing a mineral assemblage of K-feldspar + plagioclase + quartz + biotite, plane-polarized light. (**d**) Photomicrographs of the granite porphyry, showing a fine-grained granular matrix of K-feldspar + plagioclase + quartz, with K-feldspar + plagioclase + quartz phenocrysts; cross-polarized light. Abbreviations: Amp, amphibole; Bt, biotite; Kfs, K-feldspar; Pl, plagioclase; Qtz, quartz.

3. Sampling and Analytical Methods

3.1. Samples

Eight representative samples were collected along the section line that cuts across the Banzhusi granite porphyry and used for lithogeochemical analyses and petrographic studies (BZS-1, location: 34°15′47″N, 112°9′31″E; BZS-2, location: 34°16′20″N, 112°8′31″E; BZS-3, location: 34°16′21″N,

112°8′31″E; BZS-4, location: 34°17′13″N, 112°6′40″E; BZS-5 and BZS-6, location: 34°17′20″N, 112°6′17″E; BZS-7, location: 34°17′58″N, 112°6′33″E; BZS-8, location: 34°18′5″N, 112°6′32″E, BZS is an abbreviation of Banzhusi). Samples BZS-1, BZS-4, BZS-5, BZS-6, BZS-7 and BZS-8 were collected from border of the exposed intrusion and BZS-2 and BZS-3 were collected from core of the exposed intrusion. Zircon U-Pb geochronology and Hf-O isotope analyses were performed on samples BZS-1, BZS-2 and BZS-6.

3.2. Whole-Rock Geochemistry

Samples were prepared by clearing away the weathered surfaces and then grinding to ~200 mesh. Subsequently, lithogeochemical analyses were carried out using standard X-ray fluorescence (XRF), although the FeO content was analyzed with the potassium bichromate titrimetric method at the Analytical Laboratory of the Beijing Research Institute of Uranium Geology. The precision and accuracy for most major oxides were better than 2% (5% for MnO and P_2O_5). Almost all corrected values of trace elements had uncertainties within 5% (10% for Zr, Hf, Nb and Ta). The detailed analytical method was described by [54,55].

3.3. Zircon U-Pb Analysis

Samples BZS-1, BZS-2 and BZS-6 were crushed and sieved for separating zircon grains at the Langfang Honesty Geological Services Co., Ltd., China. The polished mounts were imaged under cathodoluminescence (CL).

Zircon U-Pb isotopes were analyzed on single ablation spots at the National Research Centre for Geoanalysis, Chinese Academy of Geological Sciences. A NWR193UC laser system (Elemental Scientific Lasers, Bozeman, MT, USA) operating at a wavelength of 193 nm and consisting of 35 mm spot diameters was employed for the laser ablation at a constant repetition rate of 10 Hz and a fluence of 8 J/cm^2. Each analysis incorporated a background acquisition lasting approximately 20 s (gas blank), which was followed by data acquisition from the sample for 40 s. The ablated material was carried in He and then mixed with N and Ar before being introduced to the inductively coupled plasma (ICP) source of an Agilent 7900 quadrupole inductively coupled plasma mass spectrometry (ICP-MS, Agilent, Santa Clara, CA, USA). Standard zircons 91500 (1062.4 ± 0.4 Ma) [56] and Plesovice (337.13 ± 0.37 Ma) [57] were used as the primary reference materials for the U-Pb geochronology. GJ1 [58] was used as a secondary standard. The instrumental conditions and data acquisition were similar to those described by [54]. Concordia plots and weighted mean ages were obtained using Isoplot 4.15.

3.4. Zircon Lu-Hf Analysis

In situ zircon Hf isotope measurements were performed using a New Wave UP213 laser-ablation microprobe attached to a Neptune multi-collector inductively coupled plasma mass spectrometry (MC-ICP-MS, Thermo Finnegan, San Jose, CA, USA) at the Institute of Geology, Chinese Academy of Geological Sciences, Beijing, China. The measurements were performed on the same zircon grains previously analyzed for U-Pb isotopes using a beam size of 55 mm, a laser pulse frequency of 8–10 Hz, and a laser beam energy density of 10 J/cm^2. Helium was used as an ablation carrier gas with an ablation time of 60 s. The primary reference material used for monitoring accuracy and precision of internally corrected Hf isotope ratios was zircon 91500 (0.282306 ± 0.000008 using $^{179}Hf/^{177}Hf$ = 0.7325) [59]. GJ1 (0.282000 ± 0.000005) [58] was used as a secondary standard. The instrumental conditions and data acquisition were similar to those described by [54].

Based on a decay constant value of 1.865×10^{-11} year^{-1} for ^{176}Lu [60], the present-day $^{176}Hf/^{177}Hf$ and $^{176}Lu/^{177}Hf$ of the depleted mantle are 0.28325 and 0.0384, respectively [61]. The depleted mantle Hf model age (single-stage model age, T_{DM1}) was calculated in reference to the depleted-mantle source with the present-day $^{176}Hf/^{177}Hf$ ratio of 0.28325 and $^{176}Lu/^{177}Hf$ ratio of 0.0384 [61]. The "crust" Hf model age (two-stage model, T_{DM2}) was calculated with respect to the average continental crust with a $^{176}Lu/^{177}Hf$ value of 0.015 [62].

3.5. Zircon O Isotope Analysis

In situ zircon O isotopes were measured using a Cameca 1280 microprobe via secondary ion mass spectrometry (SIMS) at the Centre for Microscopy, Characterisation and Analysis (CMCA) at the University of Western Australia. The beam size was 15 μm in diameter, and the ^{133}Cs + primary ion beam was accelerated at 10 kV, with a current intensity of −2.5 nA to −3.0 nA. Charge compensation of the Au-coated (30 μm) samples was accomplished using a normal incidence electron flood gun. The instrumental mass fractionation was corrected using the zircon reference materials Laura and Temora 2 [63]. The 91500, Penglai [64], BR266 [65] and GJ1 standards were analyzed 28 times as secondary reference materials. The analytical procedures and conditions and data acquisition were described in [66].

4. Results

4.1. Whole-Rock Geochemistry

The major and trace element analytical data of eight samples from the Banzhusi granite porphyry are listed in Table 1 and illustrated in Figures 3 and 4.

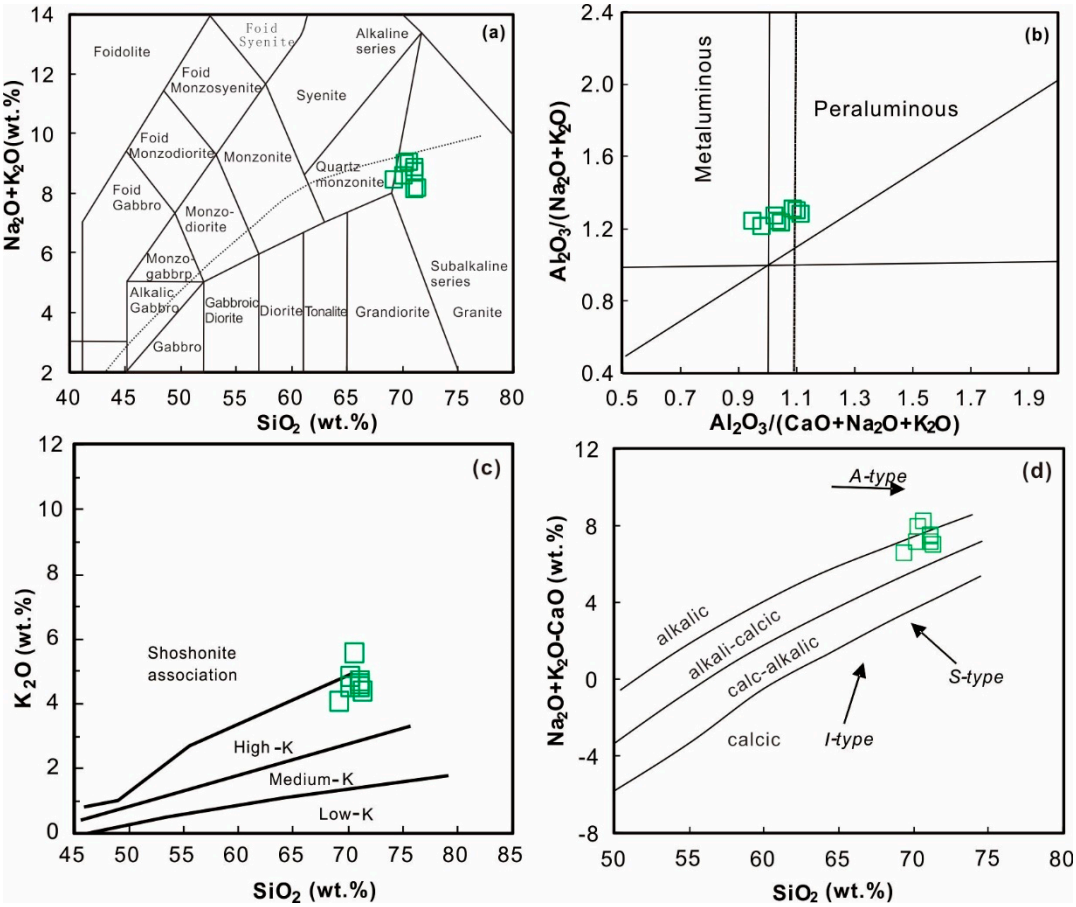

Figure 3. Geochemical classification of granitoids from the Banzhusi granite porphyry. (**a**) Total alkali-silica diagram [67], where the dashed line separating the alkaline series from the subalkaline series is from [68]. (**b**) $Al_2O_3/(Na_2O + K_2O)$ versus $Al_2O_3/(CaO + Na_2O + K_2O)$ plot [69]. (**c**) K_2O versus SiO_2 diagram (modified from [70,71]). (**d**) SiO_2 versus $Na_2O + K_2O - CaO$ [72].

Table 1. X-ray fluorescence whole-rock major oxide and trace element compositions for the Banzhusi granite porphyry.

Analysis Name	BZS-01	BZS-02	BZS-03	BZS-04	BZS-05	BZS-06	BZS-07	BZS-08
				wt. %				
SiO_2	71.3	70.2	71.1	69.2	70.2	71.1	70.6	71.1
TiO_2	0.25	0.29	0.23	0.38	0.28	0.26	0.27	0.27
Al_2O_3	14.5	15.0	14.1	14.5	14.8	14.6	15.1	14.7
ΣFe_2O_3	1.85	2.24	2.11	3.08	2.37	2.11	1.99	2.17
MnO	0.04	0.05	0.04	0.08	0.08	0.06	0.04	0.07
MgO	0.24	0.33	0.42	0.67	0.38	0.39	0.28	0.38
CaO	1.29	1.20	1.10	2.03	1.57	1.59	0.96	1.34
Na_2O	3.79	4.18	3.63	4.37	4.08	4.18	3.49	4.13
K_2O	4.41	4.87	4.54	4.11	4.54	4.72	5.61	4.65
P_2O_5	0.12	0.14	0.11	0.21	0.13	0.12	0.11	0.12
LOI	1.69	1.05	2.05	0.84	1.11	0.45	1.06	0.57
Total	99.4	99.5	99.5	99.5	99.5	99.5	99.5	99.5
K_2O/Na_2O	1.16	1.17	1.25	0.94	1.11	1.13	1.61	1.13
A/CNK	1.08	1.04	1.10	0.94	1.02	0.98	1.11	1.03
				ppm				
Li	13.4	14.4	23.1	29.9	18.7	16.9	11.2	16.5
Be	3.67	3.81	3.69	3.62	3.41	3.82	3.17	3.87
Sc	2.30	2.55	2.23	3.10	2.24	2.37	2.51	2.54
V	31.4	32.4	20.7	31.4	28.9	28.7	25.3	27.1
Cr	3.53	2.48	1.77	1.63	2.04	1.96	1.61	2.69
Co	2.21	2.15	2.34	3.24	2.54	2.12	2.22	2.56
Ni	2.10	1.77	2.28	2.21	2.39	1.87	2.29	2.97
Cu	5.23	3.79	4.51	4.58	5.14	3.85	3.83	3.95
Zn	43.8	43.8	34.9	51.6	64.9	55.9	41.6	41.0
Ga	21.7	22.2	18.5	23.9	21.5	23.1	24.8	25.9
Rb	163	172	168	131	163	169	267	180
Ba	1422	1971	1500	1460	1836	1696	1654	1704
Th	19.5	18.3	19.3	17.9	18.1	17.6	20.7	19.6
U	4.26	2.79	3.18	3.07	6.49	4.51	3.2	2.83
Nb	24.5	25.8	25.5	27.7	27.4	24.9	28.7	26.4
Ta	1.27	1.32	1.26	1.36	1.35	1.24	1.42	1.32
La	28.2	49.3	44.8	52.6	49.4	48	47.3	46
Ce	72.4	77.1	69.7	92.8	84.8	74.5	76.6	80.5
Pb	4.19	9.74	7.92	10.1	9.34	8.63	8.84	8.87

Table 1. *Cont.*

Analysis Name	BZS-01	BZS-02	BZS-03	BZS-04	BZS-05	BZS-06	BZS-07	BZS-08
Pr	13.7	34.4	27.5	35.4	32	28.9	31.1	31.6
Sr	513	708	335	609	666	615	599	583
Nd	24.5	25.8	25.5	27.7	27.4	24.9	28.7	26.4
Sm	1.96	5.09	4.05	5.31	4.78	4.28	4.66	4.65
Zr	91.7	82.9	105	69.2	79.4	77.3	97.4	88.7
Hf	2.61	2.54	3.01	2.18	2.22	2.45	2.92	2.77
Eu	0.63	1.32	0.95	1.25	1.15	1.11	1.13	1.18
Gd	1.79	4.45	3.46	4.55	3.94	3.75	4.11	3.97
Tb	0.23	0.65	0.47	0.65	0.61	0.57	0.56	0.59
Dy	1.15	2.88	2.22	3.14	2.7	2.51	2.65	2.65
Y	5.7	15.9	11.1	16.3	14.3	12.9	13.5	13.6
Ho	0.22	0.53	0.39	0.54	0.46	0.45	0.46	0.49
Er	0.62	1.48	1.11	1.48	1.35	1.3	1.26	1.35
Tm	0.11	0.22	0.19	0.24	0.21	0.20	0.21	0.22
Yb	0.82	1.65	1.26	1.66	1.42	1.39	1.4	1.47
Lu	0.13	0.22	0.20	0.23	0.20	0.20	0.19	0.22
$(La/Yb)_N$	23.3	20.3	24.2	21.5	23.6	23.5	23.0	21.3
Sr/Y	90.0	44.5	30.2	37.4	46.6	47.7	44.4	42.9
δEu	1.01	0.83	0.76	0.76	0.78	0.83	0.77	0.82

Notes: A/CNK = $Al_2O_3/(Na_2O + K_2O + CaO)$; LOI = loss on ignition; $\delta Eu = 2 \times Eu_n/(Sm_n + Gd_n)$.

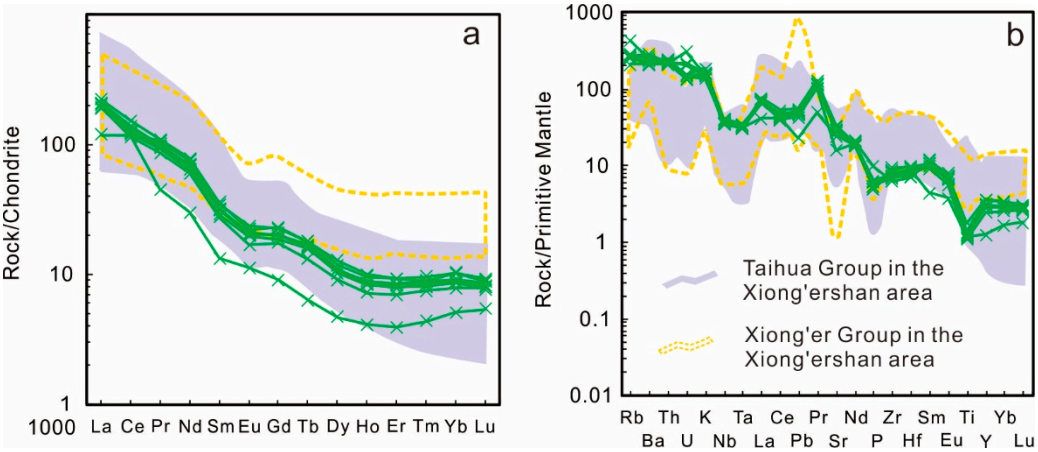

Figure 4. Chondrite-normalized rare earth element (REE) patterns (**a**) and primitive mantle-normalized multi-element diagrams (**b**) for granitoids from the Banzhusi granite porphyry. Whole-rock data for the Taihua Group and Xiong'er Group are shown for comparison [30,36]. Chondrite and primitive mantle normalizing values are from [73].

The Banzhusi granite porphyries show elevated SiO_2 (69.2 to 71.3 wt. %), Na_2O (3.5 to 4.4 wt. %), K_2O (4.1 to 5.6 wt. %), Al_2O_3 (14.1 to 15.1 wt. %), Sr (77 to 1015 ppm) and Ba (86.4 to 2293 ppm), moderate CaO (1.0 to 2.0 wt. %), K_2O/Na_2O (0.9 to 1.6), A/CNK (0.9 to 1.1) and Sr/Y (17.8 to 89.4) but low contents of MgO (0.24 to 0.67 wt. %) and FeO^T (1.85 to 3.08 ppm). These rocks are high-K alkali-calcic rocks (Figure 5) that show metaluminous features (Figure 5c). The total rare earth element (ΣREE) values are between 46.7 ppm and 257.5 ppm, with light REE (LREE)/heavy REE (HREE) ratios of 11.6 to 23.8, $(La/Yb)_N$ of 9.0 to 37.0, δCe of 0.86 to 0.93 and δEu of 0.66 to 1.1. The samples are LREE-enriched with slightly negative Eu anomalies (Figure 4).

4.2. Zircon U-Pb Ages

Sample BZS-1 has a translucent brown, euhedral and short prismatic shape zircon population, which have a length of 100 to 150 μm and are dominated by oscillatory zoning, indicating a magmatic origin. The results yield a weighted mean $^{206}Pb/^{238}U$ age of 125.1 ± 0.97 Ma (MSWD = 1.4, Figure 5b), which represents the crystallization age of the granite porphyry.

Sample BZS-2 also has a translucent light-brown to colorless, euhedral to subhedral zircon population with a length of 150–200 μm (Figure 5c). All zircons show oscillatory zoning or heterogeneous fractured features, suggesting a magmatic origin. All 13 zircons from sample BZS-2 are concordant with $^{206}Pb/^{238}U$ ages ranging from 126 to 130 Ma (Table 2), thus yielding a weighted mean age of 128.1 ± 1.2 Ma (MSWD = 1.7, Figure 5d). This weighted mean age is interpreted to represent the crystallization age of the granite porphyry.

The granite porphyry (Sample BZS-6) contains abundant euhedral- and long prismatic-shaped zircon population, which are translucent and colorless to brown. In the CL images, the euhedral- to short prismatic-shaped grains show a length of 50 - 150 μm and a length to width ratio of 3:1 to 1:1. These grains show obvious oscillatory zoning in the CL images (Figure 5e), suggesting a magmatic origin. Fifteen spots were analyzed on the representative zircon grains from BZS-6 (Table 2). These spots have concordant ages; a weighted mean $^{206}Pb/^{238}U$ age of 128.2 ± 1.3 Ma (MSWD = 2.1) was obtained, which is regarded as the crystallization age of the granite porphyry (Figure 5f).

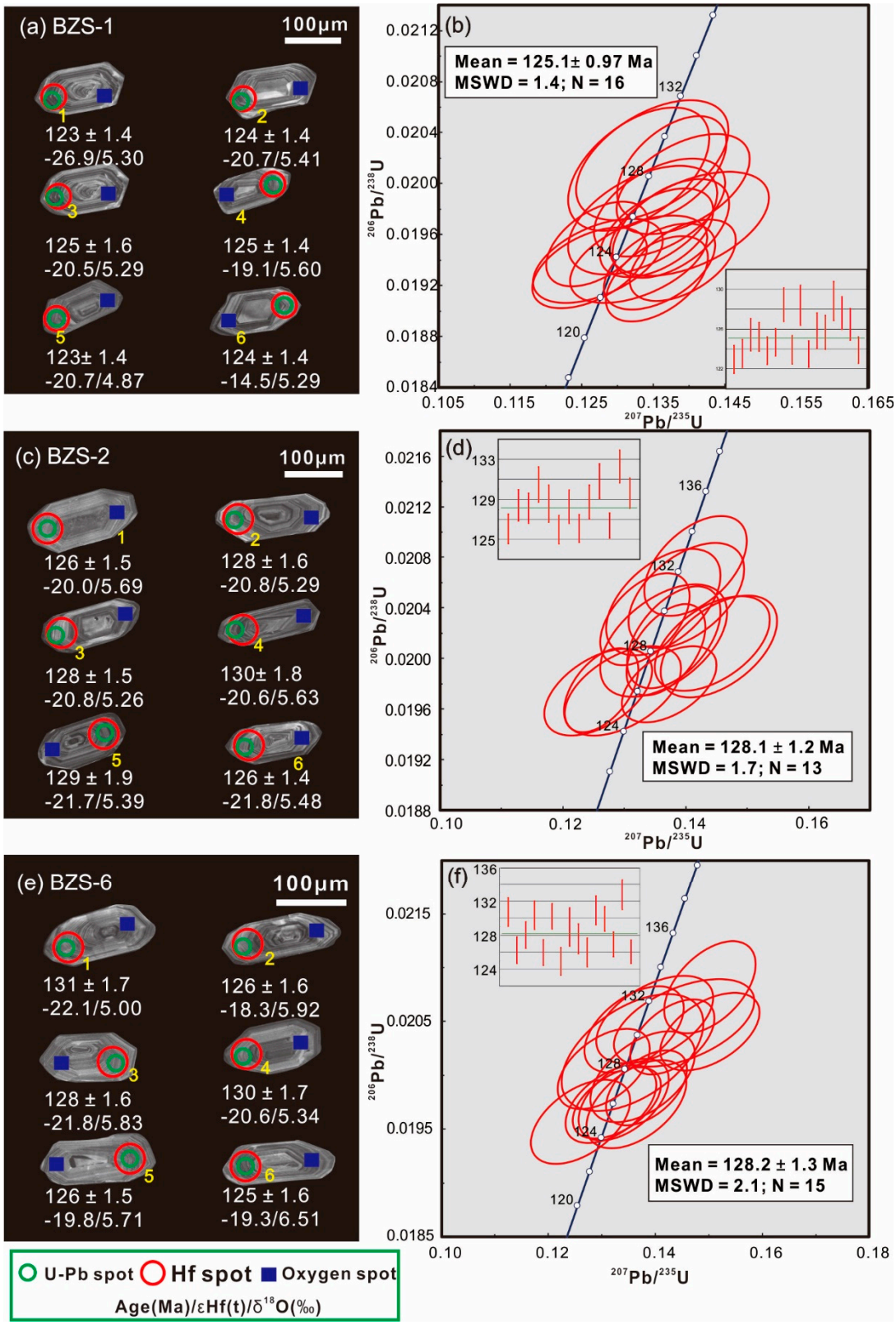

Figure 5. Cathodoluminescence images of representative analysed zircons with in situ U-Pb-Hf and O isotope data and zircon U-Pb concordia diagrams for Sample BZS-1 (**a**,**b**), Sample BZS-2 (**c**,**d**) and Sample BZS-6 (**e**,**f**) from the Banzhusi granite porphyry. Abbreviations: MSWD, weighted mean square.

Table 2. In situ LA-ICP-MS zircon U-Pb isotope compositions for the Banzhusi granite porphyry.

Analysis Name	Element (ppm)			Th/U	Isotope Ratio						Rho	Apparent Age (Ma)			
	Pb	Th	U		$^{207}Pb/^{206}Pb$	1σ	$^{207}Pb/^{235}U$	1σ	$^{206}Pb/^{238}U$	1σ		$^{207}Pb/^{235}U$	1σ	$^{206}Pb/^{238}U$	1σ
BZS-1-01	26	650	1132	0.57	0.050533	0.001859	0.135501	0.004676	0.019254	0.000221	0.3327	129	4	123	1
BZS-1-02	17	493	723	0.68	0.050386	0.001948	0.135874	0.005104	0.019350	0.000222	0.3052	129	5	124	1
BZS-1-03	14	314	578	0.54	0.050499	0.002087	0.137420	0.005368	0.019648	0.000256	0.3338	131	5	125	2
BZS-1-04	16	292	676	0.43	0.049798	0.002024	0.135477	0.005220	0.019614	0.000229	0.3026	129	5	125	1
BZS-1-06	18	673	703	0.96	0.047251	0.002256	0.127276	0.005998	0.019394	0.000218	0.2387	122	5	124	1
BZS-1-07	22	429	959	0.45	0.046912	0.001779	0.127151	0.004705	0.019528	0.000219	0.3030	122	4	125	1
BZS-1-08	19	468	767	0.61	0.049477	0.001863	0.137543	0.005017	0.020126	0.000268	0.3644	131	4	128	2
BZS-1-10	12	373	498	0.75	0.049749	0.002428	0.132929	0.006298	0.019407	0.000227	0.2463	127	6	124	1
BZS-1-11	15	324	647	0.50	0.048285	0.002301	0.132957	0.006472	0.020116	0.000319	0.3259	127	6	128	2
BZS-1-12	22	807	883	0.91	0.047237	0.001985	0.126130	0.005276	0.019340	0.000210	0.2592	121	5	123	1
BZS-1-13	13	477	504	0.95	0.049692	0.002624	0.133491	0.006855	0.019711	0.000281	0.2778	127	6	126	2
BZS-1-14	11	259	478	0.54	0.051486	0.002692	0.140042	0.007321	0.019685	0.000269	0.2618	133	7	126	2
BZS-1-15	11	316	455	0.69	0.048587	0.002513	0.134840	0.007011	0.020183	0.000311	0.2962	128	6	129	2
BZS-1-16	17	433	729	0.59	0.049802	0.002015	0.139123	0.006124	0.019995	0.000259	0.2940	132	5	128	2
BZS-1-18	16	402	688	0.58	0.049690	0.002216	0.135845	0.006020	0.019812	0.000253	0.2883	129	5	126	2
BZS-1-19	22	573	947	0.60	0.051585	0.001770	0.139085	0.004888	0.019401	0.000211	0.3096	132	4	124	1
BZS-2-01	12	226	497	0.46	0.047591	0.002391	0.129769	0.006234	0.019744	0.000235	0.2472	124	6	126	1
BZS-2-02	15	357	596	0.60	0.052107	0.002336	0.144321	0.006185	0.020117	0.000247	0.2870	137	5	128	2
BZS-2-03	25	568	1032	0.55	0.049176	0.001552	0.136777	0.004231	0.020069	0.000238	0.3835	130	4	128	2
BZS-2-05	17	405	691	0.59	0.048143	0.002172	0.136341	0.006135	0.020446	0.000279	0.3038	130	5	130	2
BZS-2-06	11	348	441	0.79	0.049214	0.002511	0.136390	0.006839	0.020143	0.000294	0.2907	130	6	129	2
BZS-2-10	12	249	532	0.47	0.046656	0.002225	0.125731	0.005767	0.019733	0.000226	0.2498	120	5	126	1
BZS-2-11	14	283	578	0.49	0.052784	0.002259	0.145380	0.006270	0.020094	0.000265	0.3058	138	6	128	2
BZS-2-13	22	578	944	0.61	0.046494	0.001507	0.126262	0.003994	0.019751	0.000219	0.3512	121	4	126	1
BZS-2-14	23	600	967	0.62	0.049827	0.001829	0.138044	0.004984	0.020168	0.000267	0.3666	131	4	129	2
BZS-2-15	11	256	455	0.56	0.049365	0.002183	0.140035	0.006208	0.020499	0.000274	0.3010	133	6	131	2
BZS-2-18	22	626	891	0.70	0.050085	0.001867	0.137304	0.005095	0.019796	0.000198	0.2694	131	5	126	1
BZS-2-19	23	507	967	0.52	0.048989	0.001794	0.141548	0.005514	0.020731	0.000260	0.3225	134	5	132	2
BZS-2-20	28	1073	1047	1.03	0.047255	0.001681	0.133325	0.004784	0.020310	0.000240	0.3288	127	4	130	2
BZS-6-01	15	377	611	0.62	0.051403	0.003105	0.145402	0.008640	0.020488	0.000267	0.2192	138	8	131	2
BZS-6-02	16	476	676	0.70	0.048784	0.001994	0.134077	0.005534	0.019774	0.000248	0.3039	128	5	126	2
BZS-6-03	15	327	618	0.53	0.046871	0.002094	0.130383	0.005702	0.020059	0.000246	0.2801	124	5	128	2
BZS-6-04	14	316	585	0.54	0.047832	0.002089	0.136039	0.006158	0.020425	0.000264	0.2853	130	6	130	2
BZS-6-05	18	376	790	0.48	0.048442	0.002439	0.131713	0.005615	0.019732	0.000238	0.2830	126	5	126	2
BZS-6-07	20	835	729	1.15	0.053378	0.002300	0.150217	0.006112	0.020405	0.000237	0.2856	142	5	130	1
BZS-6-08	11	250	469	0.53	0.046894	0.002371	0.125993	0.006130	0.019566	0.000258	0.2710	120	6	125	2
BZS-6-09	5	173	200	0.86	0.048417	0.003286	0.135670	0.008745	0.020209	0.000358	0.2752	129	8	129	2
BZS-6-10	9	211	380	0.55	0.049978	0.002451	0.137623	0.006430	0.019987	0.000278	0.2976	131	6	128	2
BZS-6-11	13	221	584	0.38	0.049855	0.002217	0.136493	0.006184	0.019732	0.000270	0.3016	130	6	126	2
BZS-6-13	9	173	381	0.45	0.049881	0.002867	0.139870	0.007189	0.020517	0.000268	0.2546	133	6	131	2
BZS-6-14	24	515	1012	0.51	0.050560	0.001887	0.143187	0.005196	0.020358	0.000230	0.3118	136	5	130	1
BZS-6-15	31	839	1316	0.64	0.050143	0.001870	0.138370	0.005008	0.019884	0.000228	0.3172	132	4	127	1
BZS-6-18	13	230	586	0.39	0.052214	0.002024	0.150191	0.005637	0.020816	0.000283	0.3617	142	5	133	2
BZS-6-20	15	325	649	0.50	0.048463	0.002006	0.132816	0.005431	0.019744	0.000218	0.2706	127	5	126	1

4.3. Zircon Lu-Hf Isotope Compositions

The Hf isotope analyses on representative zircons from BZS-1 have low $^{176}Lu/^{177}Hf$ (0.000699 to 0.001490) and homogeneous $^{176}Hf/^{177}Hf$ ratios ranging from 0.281932 to 0.282288. These results yield $\varepsilon Hf_{(t)}$ values of −21.8 to −19.2 and $f_{Lu/Hf}$ values of −0.97 to −0.96 (Figure 6, Table 3). The crustal model ages (T_{DM2}) vary from 2400 Ma to 2563 Ma (Figure 7). Zircon crystals from BZS-2 yield Lu-Hf isotope features similar to those of BZS-1, and they show low $^{176}Lu/^{177}Hf$ ratios of 0.000699 to 0.001490 with a homogeneous $^{176}Hf/^{177}Hf$ ratios of 0.281932 to 0.282288, and have $\varepsilon Hf_{(t)}$ values ranging from −26.9 to −14.4 and $f_{Lu/Hf}$ of −0.98 to −0.96. The T_{DM2} ages range from 2099 to 2889 Ma (Figure 7). Compared with BZS-1, magmatic zircons from BZS-6 yield similar $^{176}Lu/^{177}Hf$ ratios (0.000699 to 0.001490) and $^{176}Hf/^{177}Hf$ ratios (0.281932 to 0.282288), but more variable T_{DM2} ages (2099 to 2889 Ma) and $\varepsilon Hf_{(t)}$ values (−26.9 to −14.4) (Figures 6 and 7). The $f_{Lu/Hf}$ values are between −0.98 and −0.96 (Table 3).

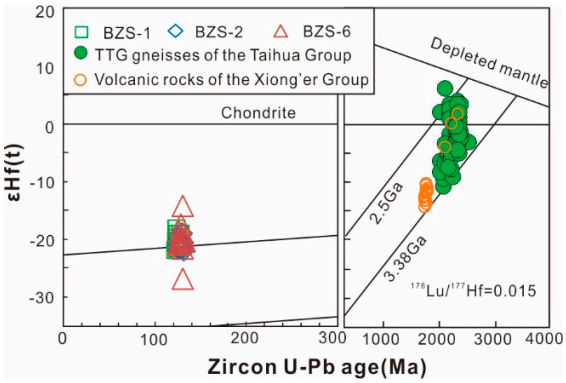

Figure 6. Variations in the initial εHf values versus the U-Pb ages of the zircons from the Banzhusi granite porphyry. Data include zircons from the Taihua Group [30] and Xiong'er Group [38].

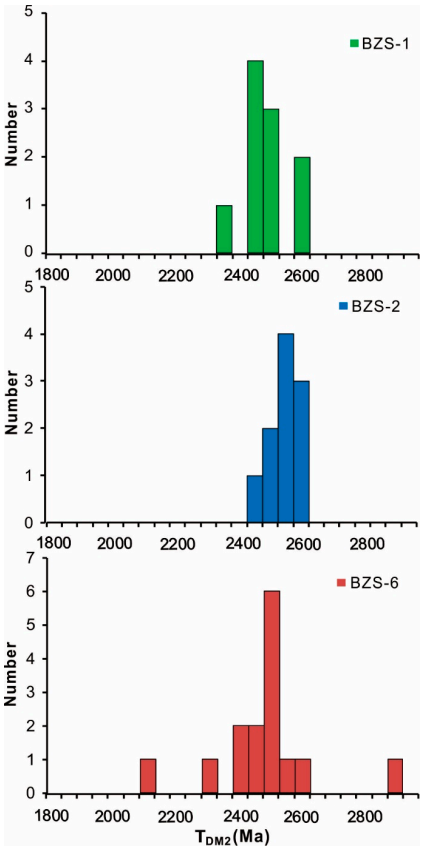

Figure 7. Histograms of the T_{DM2} ages for the zircons from the Banzhusi granite porphyry.

Table 3. In situ La-MC-ICP-MS zircon Hf isotope compositions for the Banzhusi granite porphyry.

Analysis Name	Age (Ma)	$^{176}Yb/^{177}Hf$	1σ	$^{176}Lu/^{177}Hf$	1σ	$^{176}Hf/^{177}Hf$	1σ	$(^{176}Hf/^{177}Hf)_i$	$\varepsilon_{Hf}(0)$	$\varepsilon_{Hf}(t)$	T_{DM1} (Ma)	T_{DM2} (Ma)	$f_{Lu/Hf}$
BZS-1-01	123	0.028260	0.000420	0.001024	0.000020	0.282074	0.000042	0.282072	−24.68	−22.08	1661	2580	−0.97
BZS-1-02	124	0.039650	0.000750	0.001509	0.000064	0.282182	0.000080	0.282179	−20.86	−18.28	1530	2341	−0.95
BZS-1-03	125	0.036180	0.000680	0.001283	0.000022	0.282082	0.000035	0.282079	−24.40	−21.76	1661	2562	−0.96
BZS-1-04	125	0.026860	0.000250	0.000979	0.000006	0.282115	0.000037	0.282113	−23.23	−20.58	1602	2487	−0.97
BZS-1-06	124	0.037200	0.001300	0.001352	0.000063	0.282134	0.000051	0.282131	−22.56	−19.96	1591	2447	−0.96
BZS-1-07	125	0.030820	0.000700	0.001130	0.000036	0.282153	0.000046	0.282150	−21.89	−19.26	1555	2404	−0.97
BZS-1-08	128	0.037810	0.000360	0.001344	0.000015	0.282136	0.000037	0.282133	−22.49	−19.80	1588	2440	−0.96
BZS-1-10	124	0.032400	0.001300	0.001037	0.000029	0.282112	0.000042	0.282110	−23.34	−20.71	1609	2495	−0.97
BZS-1-11	128	0.042290	0.000650	0.001538	0.000029	0.282152	0.000035	0.282148	−21.93	−19.25	1574	2405	−0.95
BZS-1-12	123	0.031900	0.001500	0.001236	0.000045	0.282118	0.000041	0.282115	−23.13	−20.53	1609	2483	−0.96
BZS-2-01	126	0.030070	0.000940	0.001093	0.000038	0.282130	0.000045	0.282127	−22.70	−20.04	1586	2454	−0.97
BZS-2-02	128	0.028100	0.001000	0.001030	0.000042	0.282106	0.000030	0.282104	−23.55	−20.83	1617	2505	−0.97
BZS-2-03	128	0.037110	0.000900	0.001329	0.000024	0.282109	0.000045	0.282106	−23.45	−20.76	1625	2500	−0.96
BZS-2-05	130	0.028900	0.002000	0.001117	0.000094	0.282112	0.000046	0.282109	−23.34	−20.58	1612	2491	−0.97
BZS-2-06	129	0.038480	0.000830	0.001476	0.000046	0.282081	0.000035	0.282077	−24.44	−21.75	1671	2563	−0.96
BZS-2-10	126	0.040800	0.002100	0.001448	0.000070	0.282082	0.000033	0.282079	−24.40	−21.77	1669	2562	−0.96
BZS-2-11	128	0.033970	0.000630	0.001295	0.000035	0.282108	0.000039	0.282105	−23.48	−20.79	1625	2502	−0.96
BZS-2-13	126	0.034670	0.000910	0.001351	0.000051	0.282100	0.000041	0.282097	−23.76	−21.12	1639	2522	−0.96
BZS-2-14	129	0.033890	0.000280	0.001410	0.000017	0.282154	0.000038	0.282151	−21.86	−19.16	1566	2400	−0.96
BZS-2-15	131	0.028660	0.000570	0.001100	0.000025	0.282073	0.000030	0.282070	−24.72	−21.95	1666	2578	−0.97
BZS-6-01	131	0.022700	0.000410	0.000699	0.000010	0.281932	0.000045	0.281930	−29.71	−26.91	1842	2889	−0.98
BZS-6-02	126	0.031930	0.000860	0.001156	0.000053	0.282111	0.000030	0.282108	−23.38	−20.71	1615	2496	−0.97
BZS-6-03	128	0.028690	0.000790	0.001032	0.000025	0.282116	0.000042	0.282114	−23.20	−20.49	1603	2483	−0.97
BZS-6-04	130	0.040900	0.002200	0.001490	0.000120	0.282154	0.000035	0.282150	−21.86	−19.13	1569	2400	−0.96
BZS-6-05	126	0.032460	0.000510	0.001135	0.000018	0.282111	0.000029	0.282108	−23.38	−20.71	1614	2496	−0.97
BZS-6-07	130	0.034600	0.001100	0.001042	0.000057	0.282288	0.000027	0.282285	−17.12	−14.36	1363	2099	−0.97
BZS-6-08	125	0.036800	0.001100	0.001368	0.000020	0.282103	0.000046	0.282100	−23.66	−21.04	1636	2516	−0.96
BZS-6-09	129	0.033890	0.000740	0.001165	0.000022	0.282136	0.000049	0.282133	−22.49	−19.77	1581	2439	−0.96
BZS-6-10	128	0.031100	0.002100	0.001224	0.000088	0.282200	0.000130	0.282197	−20.23	−17.54	1493	2298	−0.96
BZS-6-11	126	0.033600	0.002500	0.001230	0.000076	0.282135	0.000036	0.282132	−22.53	−19.87	1585	2443	−0.96
BZS-6-13	131	0.028900	0.001700	0.001035	0.000052	0.282124	0.000055	0.282121	−22.92	−20.14	1592	2464	−0.97
BZS-6-14	130	0.029170	0.000950	0.001041	0.000042	0.282081	0.000042	0.282078	−24.44	−21.68	1652	2560	−0.97
BZS-6-15	127	0.022900	0.000410	0.000795	0.000013	0.282112	0.000040	0.282110	−23.34	−20.63	1599	2492	−0.98
BZS-6-18	133	0.035560	0.000910	0.001204	0.000032	0.282114	0.000033	0.282111	−23.27	−20.47	1613	2486	−0.96
BZS-6-20	126	0.032300	0.001100	0.001163	0.000032	0.282164	0.000045	0.282161	−21.50	−18.84	1541	2378	−0.96

4.4. Zircon O Isotope Compositions

The results of the SIMS oxygen isotope analyses of zircons are presented in Figure 8 and Table 4. Zircon grains from BZS-1 have $\delta^{18}O_{zircon}$ values ranging from 4.84‰ to 5.85‰ (mean 5.31 ± 0.37‰, n = 11). Zircon grains from the BZS-2 have $\delta^{18}O_{zircon}$ values ranging from 5.26‰ to 5.75‰ and a weighted mean $\delta^{18}O_{zircon}$ of 5.51 ± 0.37‰ (n = 10). Zircon grains from BZS-6 have $\delta^{18}O_{zircon}$ values ranging from 4.94‰ to 6.51‰, displaying a weighted mean $\delta^{18}O_{zircon}$ of 5.55 ± 0.35‰ (n = 10).

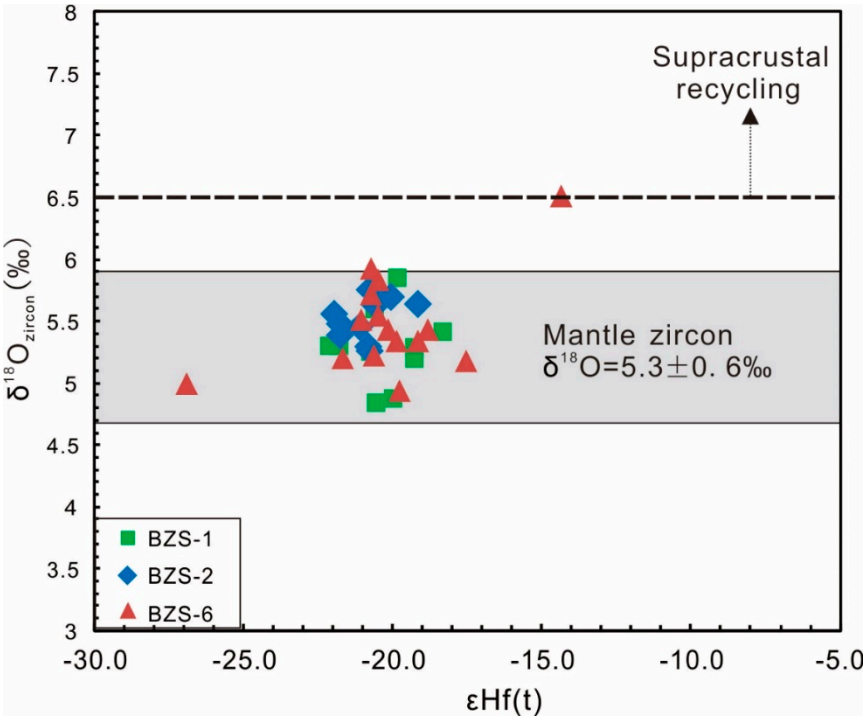

Figure 8. Combined zircon Hf-O isotope diagram from the Banzhusi granite porphyry. The range of $\delta^{18}O$ values of mantle zircons is from [74–76].

Table 4. In situ secondary ion mass spectrometry (SIMS) zircon oxygen isotope compositions for the Banzhusi granite porphyry.

Analysis Name	Raw data		Drift Corrected		SIMS Corrected Ratios		$\delta^{18}O_{zircon}$	2σ
	$^{18}O/^{16}O$	1σ Initial in Relative (%)	$^{18}O/^{16}O$	1σ	$^{18}/^{16}O$	1σ		
BZS-1-01	2.02×10^{-3}	1.11×10^{-2}	2.02×10^{-3}	2.24×10^{-7}	2.02×10^{-3}	3.71×10^{-7}	5.30	0.37
BZS-1-02	2.02×10^{-3}	1.23×10^{-2}	2.02×10^{-3}	2.48×10^{-7}	2.02×10^{-3}	3.87×10^{-7}	5.41	0.39
BZS-1-03	2.02×10^{-3}	1.18×10^{-2}	2.02×10^{-3}	2.38×10^{-7}	2.02×10^{-3}	3.80×10^{-7}	5.29	0.38
BZS-1-04	2.02×10^{-3}	7.51×10^{-3}	2.02×10^{-3}	1.52×10^{-7}	2.02×10^{-3}	3.33×10^{-7}	5.60	0.33
BZS-1-05	2.02×10^{-3}	9.52×10^{-3}	2.02×10^{-3}	1.92×10^{-7}	2.02×10^{-3}	3.53×10^{-7}	4.87	0.35
BZS-1-06	2.02×10^{-3}	1.04×10^{-2}	2.02×10^{-3}	2.10×10^{-7}	2.02×10^{-3}	3.63×10^{-7}	5.29	0.36
BZS-1-07	2.02×10^{-3}	9.64×10^{-3}	2.02×10^{-3}	1.95×10^{-7}	2.02×10^{-3}	3.55×10^{-7}	5.85	0.35
BZS-1-08	2.02×10^{-3}	1.50×10^{-2}	2.02×10^{-3}	3.03×10^{-7}	2.02×10^{-3}	4.24×10^{-7}	5.25	0.42
BZS-1-09	2.02×10^{-3}	1.06×10^{-2}	2.02×10^{-3}	2.14×10^{-7}	2.02×10^{-3}	3.65×10^{-7}	5.19	0.36
BZS-1-10	2.02×10^{-3}	1.15×10^{-2}	2.02×10^{-3}	2.32×10^{-7}	2.02×10^{-3}	3.76×10^{-7}	4.84	0.38
BZS-1-11	2.02×10^{-3}	1.39×10^{-2}	2.02×10^{-3}	2.80×10^{-7}	2.02×10^{-3}	4.07×10^{-7}	5.55	0.41
BZS-2-01	2.02×10^{-3}	6.77×10^{-3}	2.02×10^{-3}	1.37×10^{-7}	2.02×10^{-3}	3.26×10^{-7}	5.69	0.33
BZS-2-02	2.02×10^{-3}	6.87×10^{-3}	2.02×10^{-3}	1.39×10^{-7}	2.02×10^{-3}	3.27×10^{-7}	5.29	0.33
BZS-2-03	2.02×10^{-3}	1.23×10^{-2}	2.02×10^{-3}	2.47×10^{-7}	2.02×10^{-3}	3.86×10^{-7}	5.26	0.38
BZS-2-04	2.02×10^{-3}	1.79×10^{-2}	2.02×10^{-3}	3.61×10^{-7}	2.02×10^{-3}	4.67×10^{-7}	5.63	0.47
BZS-2-05	2.02×10^{-3}	1.29×10^{-2}	2.02×10^{-3}	2.60×10^{-7}	2.02×10^{-3}	3.94×10^{-7}	5.39	0.39
BZS-2-06	2.02×10^{-3}	6.74×10^{-3}	2.02×10^{-3}	1.36×10^{-7}	2.02×10^{-3}	3.26×10^{-7}	5.48	0.33
BZS-2-07	2.02×10^{-3}	9.23×10^{-3}	2.02×10^{-3}	1.86×10^{-7}	2.02×10^{-3}	3.50×10^{-7}	5.75	0.35
BZS-2-08	2.02×10^{-3}	6.72×10^{-3}	2.02×10^{-3}	1.36×10^{-7}	2.02×10^{-3}	3.26×10^{-7}	5.46	0.32
BZS-2-09	2.02×10^{-3}	1.30×10^{-2}	2.02×10^{-3}	2.63×10^{-7}	2.02×10^{-3}	3.96×10^{-7}	5.63	0.40
BZS-2-10	2.02×10^{-3}	7.79×10^{-3}	2.02×10^{-3}	1.57×10^{-7}	2.02×10^{-3}	3.35×10^{-7}	5.55	0.33
BZS-6-01	2.02×10^{-3}	9.58×10^{-3}	2.02×10^{-3}	1.93×10^{-7}	2.02×10^{-3}	3.54×10^{-7}	5.00	0.35
BZS-6-02	2.02×10^{-3}	1.09×10^{-2}	2.02×10^{-3}	2.21×10^{-7}	2.02×10^{-3}	3.70×10^{-7}	5.92	0.37
BZS-6-03	2.02×10^{-3}	1.05×10^{-2}	2.02×10^{-3}	2.11×10^{-7}	2.02×10^{-3}	3.64×10^{-7}	5.83	0.36
BZS-6-04	2.02×10^{-3}	9.24×10^{-3}	2.02×10^{-3}	1.86×10^{-7}	2.02×10^{-3}	3.50×10^{-7}	5.34	0.35
BZS-6-05	2.02×10^{-3}	8.34×10^{-3}	2.02×10^{-3}	1.68×10^{-7}	2.02×10^{-3}	3.41×10^{-7}	5.71	0.34
BZS-6-06	2.02×10^{-3}	1.07×10^{-2}	2.02×10^{-3}	2.16×10^{-7}	2.02×10^{-3}	3.67×10^{-7}	6.51	0.37
BZS-6-07	2.02×10^{-3}	7.53×10^{-3}	2.02×10^{-3}	1.52×10^{-7}	2.02×10^{-3}	3.33×10^{-7}	5.51	0.33
BZS-6-08	2.02×10^{-3}	8.72×10^{-3}	2.02×10^{-3}	1.76×10^{-7}	2.02×10^{-3}	3.44×10^{-7}	4.94	0.34
BZS-6-09	2.02×10^{-3}	1.10×10^{-2}	2.02×10^{-3}	2.22×10^{-7}	2.02×10^{-3}	3.70×10^{-7}	5.17	0.37
BZS-6-10	2.02×10^{-3}	1.06×10^{-2}	2.02×10^{-3}	2.13×10^{-7}	2.02×10^{-3}	3.65×10^{-7}	5.35	0.36
BZS-6-11	2.02×10^{-3}	1.26×10^{-2}	2.02×10^{-3}	2.54×10^{-7}	2.02×10^{-3}	3.90×10^{-7}	5.43	0.39
BZS-6-12	2.02×10^{-3}	1.33×10^{-2}	2.02×10^{-3}	2.69×10^{-7}	2.02×10^{-3}	4.00×10^{-7}	5.21	0.40
BZS-6-13	2.02×10^{-3}	9.15×10^{-3}	2.02×10^{-3}	1.85×10^{-7}	2.02×10^{-3}	3.49×10^{-7}	5.23	0.35
BZS-6-14	2.02×10^{-3}	1.34×10^{-2}	2.02×10^{-3}	2.69×10^{-7}	2.02×10^{-3}	4.00×10^{-7}	5.55	0.40
BZS-6-15	2.02×10^{-3}	1.37×10^{-2}	2.02×10^{-3}	2.77×10^{-7}	2.02×10^{-3}	4.05×10^{-7}	5.43	0.40

5. Discussion

5.1. Petrogenesis of the Banzhusi Granite Porphyry

The Banzhusi granite porphyry is characterized by high-K alkalic-calc and metaluminous to slightly peraluminous features (A/CNK ratios = 0.93–1.17, Figure 3). All samples have negative Eu anomalies (δEu = 0.661.1; Table 1) and show significant enrichments in LREEs over HREEs on normalized diagrams ($[La/Yb]_N$ = 9.0–37.0; Figure 4a). The granite porphyry samples are enriched in Rb, Ba, K, Pb, Th and U, and moderately depleted in Nb, Ta, P and Ti compared to the primitive mantle, exhibiting distinct crustal source characteristics (Figure 4b). The data mostly overlap the ranges of metamorphic rocks from the Taihua Group but show a range and pattern distinct from those of the volcanic successions from the Xiong'er Group. The geochemical data of these samples from the Banzhusi granite porphyry suggest that they were mainly generated from partial melting of the Taihua Group.

The samples BZS-1, BZS-2 and BZS-6 from the Banzhusi granite porphyry have highly evolved $\varepsilon Hf_{(t)}$ values ranging from −18.3 to −22.2, −21.8 to −19.2 and −26.9 to −14.4, which present old T_{DM2} ages ranging from 2341 to 2580 Ma, 2400 to 2563 Ma and 2099 to 2889 Ma, respectively (Table 3; Figures 6 and 7). The Hf isotope features suggest that the parental magma of the Banzhusi granite porphyry originated from an old crustal source. The Taihua Group, as the regional metamorphic crystalline basement, formed between 2.84 Ga and 2.19 Ga and presents T_{DM2} ages of 2.6–3.2 Ga [29], whereas the Paleoproterozoic Xiong'er Group volcanic rocks formed at 1.83–1.74 Ga and presents T_{DM2} ages mainly from 1.55 to 2.86 Ga [37–39,41]. Hence, we propose that the parental magma of the Banzhusi granite porphyry was dominantly derived from a crustal source in the Taihua Group based on the comparable formation ages of the Taihua Group and the T_{DM2} ages in this study.

Mantle zircons are generally accepted to have a narrow range of $\delta^{18}O$ values averaging 5.3 ± 0.6‰ (2σ) [74–76]. The $\delta^{18}O_{zircon}$ values of less than 6.5‰ form from melts that contain minor to negligible sedimentary components, whereas $\delta^{18}O_{zircon}$ values higher than 6.5‰ signify supracrustal contributions [77–82]. However, the zircon $\delta^{18}O_{zircon}$ values of samples BZS-1, BZS-2 and BZS-6 range from 4.84‰ to 5.85‰, 5.26‰ to 5.75‰ and 4.94‰ to 6.51‰ (Figure 8), respectively, indicating the contribution from the mantle or mantle-derived sources during zircon growth. The combination of zircon Hf-O isotopes of the Banzhusi granite porphyry indicates that the magma source was originally derived from ancient continental crust together with the nonnegligible involvement of mantle-derived magmas (Figures 6–8). Hence, our zircon O isotope data provide robust new evidence for the contribution of mantle-derived magmas in the origin of the Banzhusi granite porphyry.

The diagrams of $\varepsilon Hf_{(t)}$ versus $\delta^{18}O_{zircon}$ and the integrated oxygen isotope reservoir of the Earth (Figure 8) also suggest mixed sources from the Taihua Group and mantle-derived magmas. The low $\delta^{18}O_{zircon}$ values could be inherited from parental magmas. Relatively low $\delta^{18}O_{zircon}$ fluids or melts can be generated through metasomatism of the lower crust or mantle degassing in post-collisional extensional settings [83–85]. The addition of low $\delta^{18}O_{zircon}$ fluids or melts into the lower crust could accelerate the melting of the refractory Taihua Group. The required heat could be provided by underplating of hot asthenospheric mantle [86].

5.2. Relationship between the Banzhusi Granite Porphyry and Mineralization

Zircons from samples BZS-1, BZS-2 and BZS-6 of the Banzhusi granite porphyry analyzed by LA-ICP-MS in this study yielded weighted mean $^{206}Pb/^{238}U$ ages of 125.1 ± 0.97 Ma, 128.1 ± 1.2 Ma and 128.2 ± 1.3 Ma, respectively. These ages are consistent with previous zircon U-Pb ages from a recent study [18], indicating that the Banzhusi granite porphyry was formed contemporaneously with the widespread late Mesozoic magmatism in the Xiong'ershan area [21].

The late Mesozoic magmatic plutons and granite porphyries in the Xiong'ershan area include the Wuzhangshan, Haoping, Jinshanmiao, Haopinggou, Heyu and Taishanmiao granite plutons and the Leimengou, Banzhusi, Qiyugou and Shiyaogou granite porphyries. Available published

data have provided good constraints for the crystallization age of these plutons and granite porphyries [2,12,18,19,21,42,55,87–92]. The late Mesozoic magmatic event in the Xiong'ershan area principally proceeded for 60 Ma, and we suggest that three main magmatic events occurred from 177–153 Ma (Wuzhangshan pluton) [89,90], 145–125 Ma (most of the plutons and granite porphyries mentioned above except for the Wuzhangshan and Taishanmiao granite plutons) [2,18,19,21,42,55,87–92] and 125–115 Ma (Taishanmiao pluton) [12].

In this study, the zircon U-Pb data obtained from the Banzhusi granite porphyry are consistent with the regional Mo, Au, Pb, Zn, and Ag mineralization ages of 133–125 Ma [42]. Based on previous studies, three main mineralization events during the late Mesozoic have been identified in the Xiong'ershan area (i.e., 160–142 Ma, 133–125 Ma and 125–115 Ma) [21]. The formation age (128–125 Ma) of the Banzhusi granite porphyry is contemporaneous with the second episode of magmatism and metallogeny, indicating that the granite porphyry and metallogenesis were probably generated under a unified geodynamic setting.

5.3. Geodynamic Implications

To date, previous researchers have proposed four tectonic models for the late Mesozoic evolution of the EQOB. (i) During the late Mesozoic, the NCC was still subducting southward and the YC was still subducting northward beneath the Qinling orogen. Accordingly, late Mesozoic magmatism was related to the syn-collisional setting, and the subsequent post-collisional magmatism continued after the Early Cretaceous [27,93]. (ii) Li [94] and Yang et al. [95,96] proposed a second model that suggested a post-collisional evolution for the EQOB during the late Mesozoic. Therefore, late Mesozoic post-collisional granitoids were distributed in the EQOB after the Triassic collision between the NCC and YC [95–97]. (iii) The third model considered that the Palaeo-Pacific slab was subducted northwestward beneath East China during the late Mesozoic [4,48,98]. iv) Li et al. [1] proposed a new viewpoint that the collision between the NCC and YC occurred at circa 195–160 Ma, which led to the thickening of the lower continental crust, and the subsequent post-collisional magmatism continued until circa 125 Ma. Therefore, the main controversy in the above models is the shifted timing of the tectonic systems of the Qingling orogenic belt from a compressional regime to an extensional regime.

As shown in Figure 9a, few samples plot in the unfractionated M-, I- and S-type granite field (OGT), and most of the samples plot in the fractionated felsic granite field (FG). All samples plot in the post-collisional granite (post-COLG) field in Figure 9b. The above features suggest that the granite porphyry was emplaced in a post-collisional setting. The Banzhusi granite porphyry samples all plot in the post-COLG field and exhibit emplacement ages of 128–125 Ma, thus implying that the tectonic transition from a syn-collisional to a post-collisional setting could have accomplished at circa 128–125 Ma. In addition, the abovementioned zircon Hf-O isotope features (low $\varepsilon Hf_{(t)}$ and $\delta^{18}O_{zircon}$ values) of the Banzhusi granite porphyry imply lithospheric thinning with a significant input of upwelling mantle-derived materials, which resulted in the partial melting of the lower crust in this period. Dong et al. [99] proposed that the Qinling orogenic belt evolved to orogenic collapse during the Late Cretaceous to Palaeogene after the intense compression and denudation during the Late Jurassic to Early Cretaceous. Therefore, the QOB evolved orogenic collapse event is restricted to the Early Cretaceous by the emplacement age (128–125 Ma) of the Banzhusi granite porphyry.

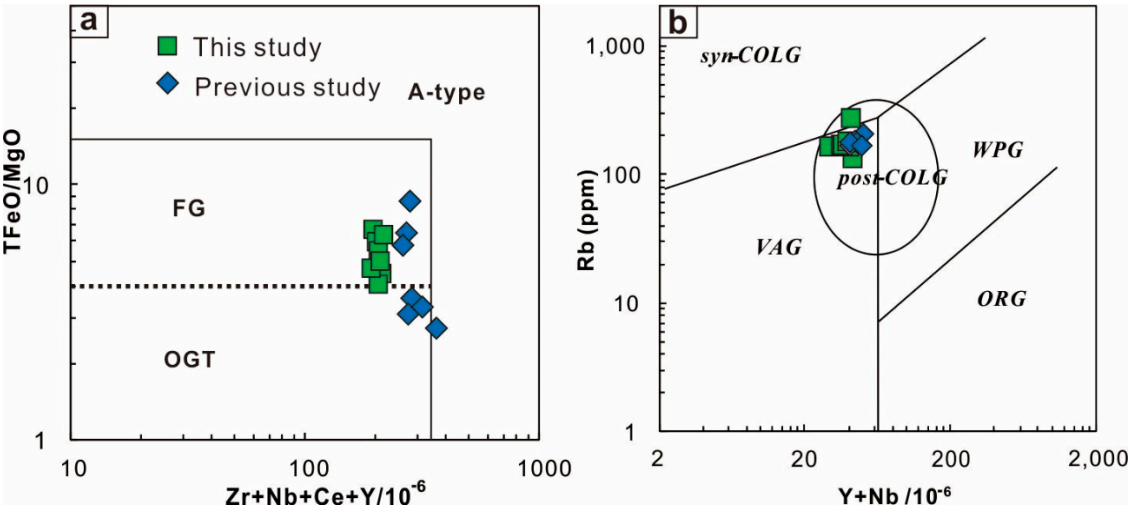

Figure 9. Geochemical discrimination diagrams of TFeO/MgO versus Zr + Nb + Ce + Y (**a**) [100] and Rb versus Y + Nb (**b**) [101] of the Banzhusi granite porphyry. A previous study was conducted by [17]. Abbreviations: A-type, A-type granites; FG, fractionated felsic granites; OGT, unfractionated M-, I- and S-type granites; syn-COLG = syn-collisional granite; post-COLG = post-collisional granite; VAG = volcanic arc granite; WPG = within-plate granite; ORG = ocean ridge granite.

6. Conclusions

(1) The zircon U-Pb data show that three samples of the Banzhusi granite porphyry yield emplacement ages of 125.1 ± 0.97 Ma, 128.1 ± 1.2 Ma and 128.2 ± 1.3 Ma.

(2) Whole-rock geochemistry and zircon Hf-O isotopes indicate that the parental magma of the Banzhusi granite porphyry was mainly sourced from partial melting of the Taihua Group mixed with non-negligible mantle-derived materials.

(3) The Early Cretaceous (128–125 Ma) granitoid magmatism in the Xiong'ershan area likely occurred due to the evolved orogenic collapse event in the Qinling orogenic belt.

Author Contributions: B.W. and X.H. carried out the whole-rock geochemistry analysis, zircon U-Pb dating and Hf-O isotope analysis and processed the data, drew the diagrams and finished the manuscript. J.L. and L.T. reviewed the manuscript and corrected the language.

Funding: This study was supported financially by the National Key Research and Development Program of China (2016YFC0600504), the Open Research Project from the State Key Laboratory of Geological Processes and Mineral Resources, China University of Geosciences (E71180115), the Fundamental Research Funds for the Central Universities (2652017276 and 2652017218) and the Geological Survey Project (121201004000172605 and 202003000000180709).

Acknowledgments: Christopher Spencer, Heejin Jeon and Yu Zhao are appreciated for their support during SIMS zircon O isotope analyses. The team members from the China University of Geosciences Beijing provided valuable assistance in the field.

Conflicts of Interest: The authors declare no conflicts of interest.

References

1. Li, N.; Chen, Y.J.; Santosh, M.; Pirajno, F. Late Mesozoic granitoids in the Qinling Orogen, Central China, and tectonic significance. *Earth-Sci. Rev.* **2018**, *182*, 141–173. [CrossRef]
2. Mao, J.; Xie, G.; Pirajno, F.; Ye, H.; Wang, Y.; Li, Y.; Xiang, J.; Zhao, H. Late Jurassic–Early Cretaceous granitoid magmatism in Eastern Qinling, central-eastern China: SHRIMP zircon U-Pb ages and tectonic implications. *Aust. J. Earth Sci.* **2010**, *57*, 51–78. [CrossRef]
3. Wang, C.; Deng, J.; Bagas, L.; Wang, Q. Zircon Hf-isotopic mapping for understanding crustal architecture and metallogenesis in the Eastern Qinling Orogen. *Gondwana Res.* **2017**, *50*, 293–310. [CrossRef]
4. Yang, F.; Xue, F.; Santosh, M.; Wang, G.; Kim, S.W.; Shen, Z.; Jia, W.; Zhang, X. Late Mesozoic magmatism in the East Qinling Orogen, China and its tectonic implications. *Geosci. Front.* **2019**, *10*, 1803–1821. [CrossRef]

5. Mao, J.; Xie, G.; Bierlein, F.; Qü, W.; Du, A.; Ye, H.; Pirajno, F.; Li, H.M.; Guo, B.; Li, Y. Tectonic implications from Re-Os dating of Mesozoic molybdenum deposits in the East Qinling-Dabie orogenic belt. *Geochim. Cosmochim. Acta* **2008**, *72*, 4607–4626. [CrossRef]
6. Stein, H.; Markey, R.; Morgan, J.; Du, A.; Sun, Y. Highly precise and accurate Re-Os ages for molybdenite from the East Qinling molybdenum belt, Shaanxi Province, China. *Econ. Geol.* **1997**, *92*, 827–835. [CrossRef]
7. Cao, M.; Yao, J.; Deng, X.; Yang, F.; Mao, G.; Mathur, R. Diverse and multistage Mo, Au, Ag-Pb-Zn and Cu deposits in the Xiong'er Terrane, East Qinling: From Triassic Cu mineralization. *Ore Geol. Rev.* **2017**, *81*, 565–574. [CrossRef]
8. Li, N.; Chen, Y.J.; Pirajno, F.; Gong, H.J.; Mao, S.D.; Ni, Z.Y. LA-ICP-MS zircon U-Pb dating, trace element and Hf isotope geochemistry of the Heyu granite batholith, eastern Qinling, central China: Implications for Mesozoic tectono-magmatic evolution. *Lithos* **2012**, *142*, 34–47. [CrossRef]
9. Li, D.; Han, J.; Zhang, S.; Yan, C.; Cao, H.; Song, Y. Temporal evolution of granitic magmas in the Luanchuan metallogenic belt, east Qinling Orogen, central China: Implications for Mo metallogenesis. *J. Asian Earth Sci.* **2015**, *111*, 663–680. [CrossRef]
10. Zhang, Y.; Cao, H.; Xu, M.; Zhang, S.; Tang, L.; Wang, S.; Pei, Q.; Cai, G.; Shen, T. Petrogenesis of the late Mesozoic highly fractionated I-type granites in the Luanchuan district: Implications for the tectono-magmatic evolution of eastern Qinling. *Geosci. J.* **2017**, *22*, 1–20. [CrossRef]
11. Zhang, Y.; Zhang, S.; Xu, M.; Jiang, X.; Li, J.; Wang, S.; Li, D.; Cao, H.; Zou, H.; Fang, Y. Geochronology, geochemistry, and Hf isotopes of the Jiudinggou molybdenum deposit, Central China, and their geological significance. *Geochem. J.* **2015**, *49*, 321–342. [CrossRef]
12. Wang, C.; Chen, L.; Bagas, L.; Lu, Y.; He, X.; Lai, X. Characterization and origin of the Taishanmiao aluminous A-type granites: Implications for Early Cretaceous lithospheric thinning at the southern margin of the North China Craton. *Int. J. Earth Sci.* **2016**, *105*, 1563–1589. [CrossRef]
13. Bao, Z.; Zeng, Q.; Zhao, T.; Yuan, Z. Geochemistry and petrogenesis of the ore-related Nannihu and Shangfanggou granite porphyries from east Qinling belt and their constraints on the molybdenum mineralization. *Acta Petrol. Sin.* **2009**, *25*, 2523–2536.
14. Bao, Z.; Xiong, M.; Li, Q. Mo-rich source and protracted crystallization of Late Mesozoic granites in the East Qinling porphyry Mo belt (central China): Constraints from zircon U/Pb ages and Hf-O isotopes. *J. Asian Earth Sci.* **2018**, *160*, 322–333. [CrossRef]
15. Bao, Z.; Wang, C.Y.; Zhao, T.; Li, C.; Gao, X. Petrogenesis of the Mesozoic granites and Mo mineralization of the Luanchuan ore field in the East Qinling Mo mineralization belt, Central China. *Ore Geol. Rev.* **2014**, *57*, 132–153. [CrossRef]
16. Bao, Z.; Sun, W.; Zartman, R.E.; Yao, J.; Gao, X. Recycling of subducted upper continental crust: Constraints on the extensive molybdenum mineralization in the Qinling-Dabie orogen. *Ore Geol. Rev.* **2017**, *81*, 451–465. [CrossRef]
17. Liang, T.; Lu, R.; Luo, Z. Geochemical features and its geologic implications of Banzhusi granitic porphyry in Xiongershan of western Henan Province. *Geol. Surv. Res.* **2016**, *39*, 15. (In Chinese)
18. Liang, T.; Bai, F.J.; Luo, Z.H.; Lu, X.X.; Lu, R.; Xu, S.T.; Cheng, J.L. LA-ICP-MS zircon U-Pb dating and its geological implications of Banzhusi granitic porphyry in Xiongershan of western Henan Province. *Northwestern Geol.* **2014**, *47*, 41–50. (In Chinese)
19. Han, Y.; Zhang, S.; Pirajno, F.; Zhou, X.; Zhao, G.; Qü, W.; Liu, S.; Zhang, J.; Liang, H.; Yang, K. U-Pb and Re-Os isotopic systematics and zircon Ce^{4+}/Ce^{3+} ratios in the Shiyaogou Mo deposit in eastern Qinling, central China: Insights into the oxidation state of granitoids and Mo (Au) mineralization. *Ore Geol. Rev.* **2013**, *55*, 29–47. [CrossRef]
20. Cao, H.W.; Zhang, S.T.; Santosh, M.; Zheng, L.; Tang, L.; Li, D.; Zhang, X.H.; Zhang, Y.H. The Luanchuan Mo-W-Pb-Zn-Ag magmatic–hydrothermal system in the East Qinling metallogenic belt, China: Constrains on metallogenesis from C-H-O-S-Pb isotope compositions and Rb-Sr isochron ages. *J. Asian Earth Sci.* **2015**, *111*, 751–780. [CrossRef]
21. Deng, J.; Gong, Q.; Wang, C.; Carranza, E.J.M.; Santosh, M. Sequence of Late Jurassic–Early Cretaceous magmatic-hydrothermal events in the Xiong'ershan region, Central China: An overview with new zircon U-Pb geochronology data on quartz porphyries. *J. Asian Earth Sci.* **2014**, *79*, 161–172. [CrossRef]

22. Hu, X.K.; Tang, L.; Zhang, S.T.; Santosh, M.; Spencer, C.J.; Zhao, Y.; Cao, H.W.; Pei, Q.M. In situ trace element and sulfur isotope of pyrite constrain ore genesis in the Shapoling molybdenum deposit, East Qinling Orogen, China. *Ore Geol. Rev.* **2019**, *105*, 123–136. [CrossRef]
23. Tang, L.; Hu, X.K.; Santosh, M.; Zhang, S.T.; Spencer, C.J.; Jeon, H.; Zhao, Y.; Cao, H.W. Multistage processes linked to tectonic transition in the genesis of orogenic gold deposit: A case study from the Shanggong lode deposit, East Qinling, China. *Ore Geol. Rev.* **2019**, *111*, 102998. [CrossRef]
24. Zhao, Y.; Pei, Q.M.; Zhang, S.T.; Guo, G.H.; Li, J.J.; Liu, W.G.; Hu, X.K.; Song, K.R.; Wang, L. Formation timing and genesis of M adiu fluorite deposit in East Qinling, China: Constraints from fluid inclusion, geochemistry, and H-O-Sr-Nd isotopes. *Geol. J.* **2019**, *2019*, 1–18. [CrossRef]
25. Wang, F.; Liu, S.A.; Li, S.; He, Y. Contrasting zircon Hf-O isotopes and trace elements between ore-bearing and ore-barren adakitic rocks in central-eastern China: Implications for genetic relation to Cu-Au mineralization. *Lithos* **2013**, *156*, 97–111. [CrossRef]
26. Wang, F.; Liu, S.A.; Li, S.; Akhtar, S.; He, Y. Zircon U-Pb ages, Hf-O isotopes and trace elements of Mesozoic high Sr/Y porphyries from Ningzhen, eastern China: Constraints on their petrogenesis, tectonic implications and Cu mineralization. *Lithos* **2014**, *200*, 299–316. [CrossRef]
27. Dong, Y.; Santosh, M. Tectonic architecture and multiple orogeny of the Qinling Orogenic Belt, Central China. *Gondwana Res.* **2016**, *29*, 1–40. [CrossRef]
28. Tang, L.; Zhang, S.T.; Yang, F.; Santosh, M.; Li, J.J.; Kim, S.W.; Hu, X.K.; Zhao, Y.; Cao, H.W. Triassic alkaline magmatism and mineralization in the Xiong'ershan area, East Qinling, China. *Geol. J.* **2019**, *54*, 143–156. [CrossRef]
29. Huang, X.L.; Wilde, S.A.; Yang, Q.J.; Zhong, J.W. Geochronology and petrogenesis of gray gneisses from the Taihua Complex at Xiong'er in the southern segment of the Trans-North China Orogen: Implications for tectonic transformation in the Early Paleoproterozoic. *Lithos* **2012**, *134*, 236–252. [CrossRef]
30. Huang, X.L.; Niu, Y.; Xu, Y.G.; Yang, Q.J.; Zhong, J.W. Geochemistry of TTG and TTG-like gneisses from Lushan-Taihua complex in the southern North China Craton: Implications for late Archean crustal accretion. *Precambrian Res.* **2010**, *182*, 43–56. [CrossRef]
31. Tang, L.; Santosh, M.; Dong, Y.; Tsunogae, T.; Zhang, S.; Cao, H. Early Paleozoic tectonic evolution of the North Qinling orogenic belt: Evidence from geochemistry, phase equilibrium modeling and geochronology of metamorphosed mafic rocks from the Songshugou ophiolite. *Gondwana Res.* **2016**, *30*, 48–64. [CrossRef]
32. Tang, L.; Santosh, M.; Dong, Y. Tectonic evolution of a complex orogenic system: Evidence from the northern Qinling belt, central China. *J. Asian Earth Sci.* **2015**, *113*, 544–559. [CrossRef]
33. Yu, X.; Liu, J.; Li, C.; Chen, S.; Dai, Y. Zircon U-Pb dating and Hf isotope analysis on the Taihua Complex: Constraints on the formation and evolution of the Trans-North China Orogen. *Precambrian Res.* **2013**, *230*, 31–44. [CrossRef]
34. Xu, X.; Griffin, W.L.; Ma, X.; O'Reilly, S.Y.; He, Z.; Zhang, C. The Taihua group on the southern margin of the North China craton: Further insights from U-Pb ages and Hf isotope compositions of zircons. *Mineral. Petrol.* **2009**, *97*, 43. [CrossRef]
35. He, Y.; Zhao, G.; Sun, M.; Xia, X. SHRIMP and LA-ICP-MS zircon geochronology of the Xiong'er volcanic rocks: Implications for the Paleo-Mesoproterozoic evolution of the southern margin of the North China Craton. *Precambrian Res.* **2009**, *168*, 213–222. [CrossRef]
36. He, Y.; Zhao, G.; Sun, M. Geochemical and isotopic study of the Xiong'er volcanic rocks at the southern margin of the North China Craton: Petrogenesis and tectonic implications. *J. Geol.* **2010**, *118*, 417–433. [CrossRef]
37. Peng, P.; Zhai, M.; Ernst, R.E.; Guo, J.; Liu, F.; Hu, B. A 1.78 Ga large igneous province in the North China craton: The Xiong'er Volcanic Province and the North China dyke swarm. *Lithos* **2008**, *101*, 260–280. [CrossRef]
38. Wang, X.L.; Jiang, S.Y.; Dai, B.Z. Melting of enriched Archean subcontinental lithospheric mantle: Evidence from the ca. 1760 Ma volcanic rocks of the Xiong'er Group, southern margin of the North China Craton. *Precambrian Res.* **2010**, *182*, 204–216. [CrossRef]
39. Wang, C.; He, X.; Carranza, E.J.M.; Cui, C. Paleoproterozoic volcanic rocks in the southern margin of the North China Craton, central China: Implications for the Columbia supercontinent. *Geosci. Front.* **2019**, *10*, 1543–1560. [CrossRef]

40. Zhao, T.P.; Zhou, M.F.; Zhai, M.; Xia, B. Paleoproterozoic rift-related volcanism of the Xiong'er Group, North China craton: Implications for the breakup of Columbia. *International Geol. Rev.* **2002**, *44*, 336–351. [CrossRef]
41. Zhao, T.; Zhai, M.; Xia, B.; Li, H.; Zhang, Y.; Wan, Y. Zircon U-Pb SHRIMP dating for the volcanic rocks of the Xiong'er Group: Constraints on the initial formation age of the cover of the North China Craton. *Chin. Sci. Bull.* **2004**, *49*, 2495–2502. [CrossRef]
42. Zhao, T.; Meng, L.; Gao, X.; Jin, C.; Wu, Q.; Bao, Z. Late Mesozoic felsic magmatism and Mo-Au-Pb-Zn mineralization in the southern margin of the North China Craton: A review. *J. Asian Earth Sci.* **2018**, *161*, 103–121. [CrossRef]
43. Chen, Y.J.; Pirajno, F.; Qi, J.P. The Shanggong gold deposit, Eastern Qinling Orogen, China: Isotope geochemistry and implications for ore genesis. *J. Asian Earth Sci.* **2008**, *33*, 252–266. [CrossRef]
44. Mao, J.; Goldfarb, R.J.; Zhang, Z.; Xu, W.; Qiu, Y.; Deng, J. Gold deposits in the Xiaoqinling–Xiong'ershan region, Qinling Mountains, central China. *Miner. Depos.* **2002**, *37*, 306–325. [CrossRef]
45. Deng, X.H.; Chen, Y.J.; Pirajno, F.; Li, N.; Yao, J.M.; Sun, Y.L. The geology and geochronology of the Waifangshan Mo-quartz vein cluster in eastern Qinling, China. *Ore Geol. Rev.* **2017**, *81*, 548–564. [CrossRef]
46. Deng, X.H.; Chen, Y.J.; Bagas, L.; Zhou, H.Y.; Yao, J.M.; Zheng, Z.; Wang, P. Isotope (S-Sr-Nd-Pb) constraints on the genesis of the ca. 850 Ma tumen Mo–F deposit in the Qinling Orogen, China. *Precambrian Res.* **2015**, *266*, 108–118. [CrossRef]
47. Huang, D.; Hou, Z.; Yang, Z.; Li, Z.; Xu, D. Geological and geochemical characteristics, metallogenetic mechanism and tectonic setting of carbonatite vein-type Mo (Pb) deposits in the East Qinling molybdenum ore belt. *Acta Geol. Sin.* **2009**, *83*, 1968–1984.
48. Mao, J.; Pirajno, F.; Xiang, J.; Gao, J.; Ye, H.; Li, Y.; Guo, B. Mesozoic molybdenum deposits in the east Qinling-Dabie orogenic belt: Characteristics and tectonic settings. *Ore Geol. Rev.* **2011**, *43*, 264–293. [CrossRef]
49. Chen, Y.J.; Pirajno, F.; Li, N.; Guo, D.S.; Lai, Y. Isotope systematics and fluid inclusion studies of the Qiyugou breccia pipe-hosted gold deposit, Qinling Orogen, Henan province, China: Implications for ore genesis. *Ore Geol. Rev.* **2009**, *35*, 245–261. [CrossRef]
50. Fan, H.R.; Hu, F.F.; Wilde, S.A.; Yang, K.F.; Jin, C.W. The Qiyugou gold-bearing breccia pipes, Xiong'ershan region, central China: Fluid-inclusion and stable-isotope evidence for an origin from magmatic fluids. *Int. Geol. Rev.* **2011**, *53*, 25–45. [CrossRef]
51. Tian, Y.; Sun, J.; Ye, H.; Mao, J.; Wang, X.; Bi, M.; Xia, X. Genesis of the Dianfang breccia-hosted gold deposit, western Henan Province, China: Constraints from geology, geochronology and geochemistry. *Ore Geol. Rev.* **2017**, *91*, 963–980. [CrossRef]
52. Li, Z.K.; Li, J.W.; Zhao, X.F.; Zhou, M.F.; Selby, D.; Bi, S.J.; Sui, J.X.; Zhao, Z.J. Crustal-extension Ag-Pb-Zn veins in the Xiong'ershan District, Southern North China craton: Constraints from the Shagou deposit. *Econ. Geol.* **2013**, *108*, 1703–1729. [CrossRef]
53. Li, Z.K.; Li, J.W.; Cooke, D.R.; Danyushevsky, L.; Zhang, L.; O'Brien, H.; Lahaye, Y.; Zhang, W.; Xu, H.J. Textures, trace elements, and Pb isotopes of sulfides from the Haopinggou vein deposit, southern North China Craton: Implications for discrete Au and Ag-Pb-Zn mineralization. *Contrib. Mineral. Petrol.* **2016**, *171*, 99. [CrossRef]
54. Pei, Q.M.; Zhang, S.T.; Hayashi, K.I.; Cao, H.W.; Li, D.; Tang, L.; Hu, X.K.; Li, H.X.; Fang, D.R. Permo-Triassic granitoids of the Xing'an-Mongolia segment of the Central Asian Orogenic Belt, Northeast China: Age, composition, and tectonic implications. *Int. Geol. Rev.* **2018**, *60*, 1172–1194. [CrossRef]
55. Cao, J.; Ye, H.; Chen, X.; He, W.; Wang, P. Geochemistry, zircon U-Pb age, and Lu-Hf isotope of the granite porphyry in Leimengou Mo deposit in the east Qinling Molybdenum ore belt, China. *Minerals* **2018**, *8*, 293. [CrossRef]
56. Wiedenbeck, M.; Hanchar, J.M.; Peck, W.H.; Sylvester, P.; Valley, J.; Whitehouse, M.; Kronz, A.; Morishita, Y.; Nasdala, L.; Fiebig, J. Further characterisation of the 91500 zircon crystal. *Geostand. Geoanalytical Res.* **2004**, *28*, 9–39. [CrossRef]
57. Sláma, J.; Košler, J.; Condon, D.J.; Crowley, J.L.; Gerdes, A.; Hanchar, J.M.; Horstwood, M.S.; Morris, G.A.; Nasdala, L.; Norberg, N. Plešovice zircon—A new natural reference material for U-Pb and Hf isotopic microanalysis. *Chem. Geol.* **2008**, *249*, 1–35. [CrossRef]
58. Morel, M.L.A.; Nebel, O.; Nebel-Jacobsen, Y.J.; Miller, J.S.; Vroon, P.Z. Hafnium isotope characterization of the GJ-1 zircon reference material by solution and laser-ablation MC-ICPMS. *Chem. Geol.* **2008**, *255*, 231–235. [CrossRef]

59. Woodhead, J.D.; Hergt, J.M. A preliminary appraisal of seven natural zircon reference materials for in situ Hf isotope determination. *Geostand. Geoanalytical Res.* **2005**, *29*, 183–195. [CrossRef]
60. Scherer, E.; Münker, C.; Mezger, K. Calibration of the lutetium-hafnium clock. *Science* **2001**, *293*, 683–687. [CrossRef]
61. Griffn, W.L.; Pearson, N.J.; Belousova, E.; Jackson, S.E.; van Achterbergh, E.; O'Reilly, S.Y.; Shee, S.R. The Hf isotope composition of cratonic mantle: LAM-MC-ICPMS analysis of zircon megacrysts in kimberlites. *Geochim. Cosmochim. Acta* **2000**, *64*, 133–147. [CrossRef]
62. Griffin, W.L.; Wang, X.; Jackson, S.E.; Pearson, N.J.; O'Reilly, S.Y.; Xu, X.; Zhou, X. Zircon chemistry and magma mixing, SE China: In-situ analysis of Hf isotopes, Tonglu and Pingtan igneous complexes. *Lithos* **2002**, *61*, 237–269. [CrossRef]
63. Black, L.P.; Kamo, S.L.; Allen, C.M.; Davis, D.W.; Aleinikoff, J.N.; Valley, J.W.; Mundil, R.; Campbell, I.H.; Korsch, R.J.; Williams, I.S. Improved $^{206}Pb/^{238}U$ microprobe geochronology by the monitoring of a trace-element-related matrix effect; SHRIMP, ID-TIMS, ELA-ICP-MS and oxygen isotope documentation for a series of zircon standards. *Chem. Geol.* **2004**, *205*, 115–140. [CrossRef]
64. Li, X.H.; Long, W.G.; Li, Q.L.; Liu, Y.; Zheng, Y.F.; Yang, Y.H. Penglai zircon megacrysts: A potential new working reference material for microbeam determination of Hf-O isotopes and U-Pb age. *Geostand. Geoanalytical Res.* **2010**, *34*, 117–134. [CrossRef]
65. Stern, R.A. *A New Isotopic and Trace-Element Standard for the Ion Microprobe: Preliminary Thermal Ionization Mass Spectrometry (TIMS) U-Pb and Electron-Microprobe Data*; Natural Resources Canada, Geological Survey of Canada: Ottawa, Australia, 2001.
66. Spencer, C.J.; Cavosie, A.J.; Raub, T.D.; Rollinson, H.; Jeon, H.; Searle, M.P.; Miller, J.A.; McDonald, B.J.; Evans, N.J. Evidence for melting mud in Earth's mantle from extreme oxygen isotope signatures in zircon. *Geology* **2017**, *45*, 975–978. [CrossRef]
67. Middlemost, E.A. Naming materials in the magma/igneous rock system. *Earth-Sci. Rev.* **1994**, *37*, 215–224. [CrossRef]
68. Irvine, T.; Baragar, W. A guide to the chemical classification of the common volcanic rocks. *Can. J. Earth Sci.* **1971**, *8*, 523–548. [CrossRef]
69. Rudnick, R.L.; Gao, S. Composition of the continental crust. *Treatise Geochem.* **2003**, *3*, 659.
70. Gill, J.B. *Orogenic Andesites and Plate Tectonics*; Springer Science & Business Media: Berlin, Germany, 2012.
71. Peccerillo, A.; Taylor, S. Geochemistry of Eocene calc-alkaline volcanic rocks from the Kastamonu area, northern Turkey. *Contrib. Mineral. Petrol.* **1976**, *58*, 63–81. [CrossRef]
72. Frost, B.R.; Barnes, C.G.; Collins, W.J.; Arculus, R.J.; Ellis, D.J.; Frost, C.D. A geochemical classification for granitic rocks. *J. Petrol.* **2001**, *42*, 2033–2048. [CrossRef]
73. Sun, S.S.; McDonough, W.F. Chemical and isotopic systematics of oceanic basalts: Implications for mantle composition and processes. *Geol. Soc., Lond., Spec. Publ.* **1989**, *42*, 313–345. [CrossRef]
74. Valley, J.; Lackey, J.; Cavosie, A.; Clechenko, C.; Spicuzza, M.; Basei, M.; Bindeman, I.; Ferreira, V.; Sial, A.; King, E. 4.4 billion years of crustal maturation: Oxygen isotope ratios of magmatic zircon. *Contrib. Mineral. Petrol.* **2005**, *150*, 561–580. [CrossRef]
75. Valley, J. Oxygen isotopes in zircon. *Rev. Mineral. Geochem.* **2003**, *53*, 343–385. [CrossRef]
76. Valley, J.W.; Kinny, P.D.; Schulze, D.J.; Spicuzza, M.J. Zircon megacrysts from kimberlite: Oxygen isotope variability among mantle melts. *Contrib. Mineral. Petrol.* **1998**, *133*, 1–11. [CrossRef]
77. Cavosie, A.; Valley, J.; Wilde, S. Magmatic $\delta^{18}O$ in 4400–3900 Ma detrital zircons: A record of the alteration and recycling of crust in the Early Archean. *Earth Planet. Sci. Lett.* **2005**, *235*, 663–681. [CrossRef]
78. Fu, B.; Mernagh, T.P.; Kita, N.T.; Kemp, A.I.; Valley, J.W. Distinguishing magmatic zircon from hydrothermal zircon: A case study from the Gidginbung high-sulphidation Au-Ag-(Cu) deposit, SE Australia. *Chem. Geol.* **2009**, *259*, 131–142. [CrossRef]
79. Hawkesworth, C.; Kemp, A. Using hafnium and oxygen isotopes in zircons to unravel the record of crustal evolution. *Chem. Geol.* **2006**, *226*, 144–162. [CrossRef]
80. Hawkesworth, C.J.; Dhuime, B.; Pietranik, A.; Cawood, P.; Kemp, A.; Storey, C. The generation and evolution of the continental crust. *J. Geol. Soc.* **2010**, *167*, 229–248. [CrossRef]
81. Kemp, A.; Hawkesworth, C.; Foster, G.; Paterson, B.; Woodhead, J.; Hergt, J.; Gray, C.; Whitehouse, M. Magmatic and crustal differentiation history of granitic rocks from Hf-O isotopes in zircon. *Science* **2007**, *315*, 980–983. [CrossRef]

82. Kemp, A.; Hawkesworth, C.; Paterson, B.; Kinny, P. Episodic growth of the Gondwana supercontinent from hafnium and oxygen isotopes in zircon. *Nature* **2006**, *439*, 580. [CrossRef]
83. Eiler, J.M.; Farley, K.A.; Valley, J.W.; Stolper, E.M.; Hauri, E.H.; Craig, H. Oxygen isotope evidence against bulk recycled sediment in the mantle sources of Pitcairn Island lavas. *Nature* **1995**, *377*, 138. [CrossRef]
84. Eiler, J.M.; McInnes, B.; Valley, J.W.; Graham, C.M.; Stolper, E.M. Oxygen isotope evidence for slab-derived fluids in the sub-arc mantle. *Nature* **1998**, *393*, 777. [CrossRef]
85. Macpherson, C.G.; Dreher, S.T.; Thirlwall, M.F. Adakites without slab melting: High pressure differentiation of island arc magma, Mindanao, the Philippines. *Earth Planet. Sci. Lett.* **2006**, *243*, 581–593. [CrossRef]
86. Xue, S.; Xu, Y.; Ling, M.X.; Kang, Q.Q.; Jiang, X.Y.; Sun, S.J.; Wu, K.; Zhang, Z.K.; Luo, Z.B.; Liu, Y.L. Geochemical constraints on genesis of Paleoproterozoic A-type granite in the south margin of North China Craton. *Lithos* **2018**, *304*, 489–500. [CrossRef]
87. Gao, X.Y.; Zhao, T.P.; Bao, Z.W.; Yang, A.Y. Petrogenesis of the early Cretaceous intermediate and felsic intrusions at the southern margin of the North China Craton: Implications for crust–mantle interaction. *Lithos* **2014**, *206*, 65–78. [CrossRef]
88. Yao, J.M.; Zhao, T.P.; Li, J.; Sun, Y.; Yuan, Z.L.; Chen, W.; Han, J. Molybdenite Re-Os age and zircon U-Pb age and Hf isotope geochemistry of the Qiyugou gold system, Henan Province. *Acta Petrol. Sin.* **2009**, *25*, 374–384. (In Chinese)
89. Lai, X.R. Mesozoic Granitoids Constraints on Gold Mineralization in the Xiong'ershan-Waifangshan Region. Master's Thesis, China University of Geosciences Beijing, Beijing, China, 2015. (In Chinese).
90. Nie, Z.R.; Wang, X.X.; Ke, C.H.; Yang, Y.; Lv, X.Q. Age, geochemistry and petrogenesis of Huashan granitonid pluton on the southern margin of the North China Block. *Geol. Bull. China* **2015**, *34*, 1502–1516. (In Chinese)
91. Xiao, E.; Jian, H.; Zunzhong, Z.; BaoZhang, D.; YanFen, W.; HaiYong, L. Petrogeochemistry, zircon U-Pb dating and Lu-Hf isotopic compositions of the Haoping and Jinshanmiao granites from the Huashan complex batholith in eastern Qinling Orogen. *Acta Petrol. Sin.* **2012**, *28*, 4031–4046. (In Chinese)
92. Li, Y.; Mao, J.; Liu, D.; Wang, Y.; Wang, Z.; Wang, Y.; Li, X.; Zhang, Z.; Guo, B. SHRIMP zircon U-Pb and molybdenite Re-Os datings for the Leimengou porphyry molybdenum deposit, western Henan and its geological implication. *Geol. Rev.* **2006**, *52*, 122–131. (In Chinese)
93. Zhang, Z.; Yang, X.; Dong, Y.; Zhu, B.; Chen, D. Molybdenum deposits in the eastern Qinling, central China: Constraints on the geodynamics. *Int. Geol. Rev.* **2011**, *53*, 261–290. [CrossRef]
94. Li, Z.K. Metallogenesis of the Silver-Lead-Zinc Deposits Along the Southern Margin of the North China Craton. Ph.D. Thesis, China University of Geosciences Wuhan, Wuhan, China, 2013. (In Chinese).
95. Yang, Y.F.; Chen, Y.J.; Pirajno, F.; Li, N. Evolution of ore fluids in the Donggou giant porphyry Mo system, East Qinling, China, a new type of porphyry Mo deposit: Evidence from fluid inclusion and H-O isotope systematics. *Ore Geol. Rev.* **2015**, *65*, 148–164. [CrossRef]
96. Yang, Y.F.; Li, N.; Chen, Y.J. Fluid inclusion study of the Nannihu giant porphyry Mo-W deposit, Henan Province, China: Implications for the nature of porphyry ore-fluid systems formed in a continental collision setting. *Ore Geol. Rev.* **2012**, *46*, 83–94. [CrossRef]
97. Harris, N.B.; Pearce, J.A.; Tindle, A.G. Geochemical characteristics of collision-zone magmatism. *Geol. Soc., Lond., Spec. Publ.* **1986**, *19*, 67–81. [CrossRef]
98. Pirajno, F.; Zhou, T. Intracontinental porphyry and porphyry-skarn mineral systems in Eastern China: Scrutiny of a special case "Made-in-China". *Econ. Geol.* **2015**, *110*, 603–629. [CrossRef]
99. Dong, Y.; Yang, Z.; Liu, X.; Sun, S.; Li, W.; Cheng, B.; Zhang, F.; Zhang, X.; He, D.; Zhang, G. Mesozoic intracontinental orogeny in the Qinling Mountains, central China. *Gondwana Res.* **2016**, *30*, 144–158. [CrossRef]
100. Whalen, J.B.; Currie, K.L.; Chappell, B.W. A-type granites: Geochemical characteristics, discrimination and petrogenesis. *Contrib. Mineral. Petrol.* **1987**, *95*, 407–419. [CrossRef]
101. Pearce, J. Sources and settings of granitic rocks. *Episodes* **1996**, *19*, 120–125.